

POLITECNICO DI TORINO

Master's Degree in Physics of Complex Systems



Master's Degree Thesis

Self-Organized Molecular Sorting on Fluid Membranes

Supervisors

Prof. Luca DALL'ASTA

Prof. Andrea GAMBA

Candidate

Riccardo ROSSETTO

July 2022

Summary

Molecular sorting is a fundamental process responsible for the organization of matter in eukaryotic cells. It allows cells to counteract the homogenizing effect of diffusion, and to maintain different functional properties in appropriated membrane subregions. A recent phenomenological theory proposes that this process could emerge from two main physical phenomena, (*a*) phase separation induced by molecular self-aggregation and (*b*) vesicle nucleation due to a coupling between particle presence and membrane spontaneous curvature. To further explore this theory preceding works introduced a minimal lattice gas model, in which the membrane is described as a flat two dimensional surface, and investigated its stationary state numerically. In this work the model is extended to take place on a fluid membrane. This allows to introduce an interaction between the presence of particles and the surface spontaneous curvature, which couples the molecular sorting process with surface fluctuations.

The membrane is described using the Helfrich Hamiltonian, which allows to do some theoretical predictions, and simulated employing a Dynamically Triangulated Monte Carlo (DTMC) model. The latter is used to simulate both thermal fluctuations and diffusion of the surface, onto which particles behaving accordingly to a Markov process of insertion, domain aggregation and extraction are inserted and coupled with curvature. Various properties of both the membrane and the distillation process are investigated at different values of the particle curvature coupling and the elastic constant.

Table of Contents

1	Introduction	1
2	Self-Organized Molecular Sorting	3
2.1	Reaction Rate Theory	3
2.2	Aggregation	5
2.2.1	Island Growth Model	7
2.3	Phenomenological Theory	8
2.4	Lattice gas Model	12
3	Field-Theoretic Description of a Fluid Membrane	14
3.1	Differential geometry and total surface area	14
3.2	Curvature	17
3.3	Continuous Model of a fluid membrane	19
3.4	The Crumpling transition	22
3.5	Curvature Instability	25
4	Dynamically Triangulated Monte Carlo	28
4.1	Triangulated Surface Model	28
4.2	Monte Carlo Procedure	31
4.3	Technical Remarks	34
4.4	Coupling with particles	34
4.5	Model Implementation	35
5	Results and Discussion	38
5.1	Domain Distance frequency density	40
	Bibliography	43

Chapter 1

Introduction

Molecular sorting is a major mechanism regulating the organization of cellular matter in eukaryotic cells. It allows cells to counteract the homogenizing effect of diffusion, by the sorting and distillation of specific proteins in submicrometric vesicles. Such vesicles, after the detach from the membrane, are then transported towards appropriate destinations by active mechanisms [1, 2].

A phenomenological theory has recently been introduced [3] and extended [4], proposing that molecular sorting may emerge from two main physical phenomena, (*a*) phase separation induced by molecular self-aggregation and (*b*) vesicle nucleation originating from a coupling between the molecules and the membrane curvature.

In both these works a spatially homogeneous probability of nucleation of sorting domains is considered. It has however been observed that sorting domains may cluster in "hotspots" or "nucleation organizers" [5]. This kind of spatial correlation may be due to effects that take place only onto a fluctuating surface. The numerical works of the preceding papers [3, 4] both took place on a flat lattice, so in order to investigate this possibility, and more in general to investigate how the surface fluctuations and the sorting process influence each other, in this work the model is simulated onto a fluctuating membrane.

It is widely recognized in the literature that fluid membranes are well described, at a mesoscopic scale, in a field-theoretic framework, using a phenomenological elastic functional, the Helfrich Hamiltonian [6, 7, 8]. This framework allows to make theoretical predictions about the behaviour of the membrane, that can be confronted with computational results. To simulate fluid membranes, the computational tool of Dynamically Triangulated Monte Carlo models (DTMC) is used. In this context two Monte Carlo moves are used: (1) vertex moves, which randomly displace vertices within a cube in space and (2) link flips, which select a random bond and substitute it with another tether connecting two previously unconnected vertices. The two moves simulate respectively thermal fluctuations and diffusion. This method was largely used to simulate fluid membranes [9, 10, 11, 12, 13, 14].

In order to investigate computationally the molecular sorting phenomenological theory onto a fluid membrane, particles behaving according to the Markov process already used in [3, 4] were inserted onto the fluid membrane model described above. The new element introduced is a coupling between the particles and the membrane curvature.

Chapter 2

Self-Organized Molecular Sorting

As explained in the introduction the main idea of this work is to extend the model proposed in [3, 4], which is defined on a two dimensional flat lattice, on a fluctuating two dimensional surface, embedded in a three dimensional euclidean space. In the present chapter, first two auxiliary concepts from nonequilibrium physics are reviewed [15] and then the model of self-organized molecular sorting is explained.

2.1 Reaction Rate Theory

Reaction rate theory studies diffusion-controlled reactions. In such processes two constituents react as soon as they are within an interaction radius, so the evolution of this reaction is determined by the timescale with which diffusion brings the reactants in proximity. The goal of this theory is to determine at which rate diffusing particles hit an absorbing object. Starting the description in $d = 3$, we have an object surrounded by a gas of non interacting particles, each of which is absorbed whenever it hits the surface of the object (Fig.2.1).

The reaction rate is defined as the steady-state diffusive flux to the object \mathcal{B} . To find it we need to solve the diffusion equation for the concentration $n(\vec{r}, t)$ outside the object, with absorption on its boundary $\partial\mathcal{B}$. We choose a spatially uniform initial condition for the density outside the object, so we have:

$$\frac{\partial n}{\partial t} = D\nabla^2 n \tag{2.1}$$

with $n(\vec{r}, 0) = \bar{n}$, and $n(\vec{r} \in \partial\mathcal{B}, t) = n_0$. In $d = 3$ an important simplification is present, since the diffusion is **transient** the concentration reaches a **steady state**, because the depletion of particles from the region near \mathcal{B} is balanced from

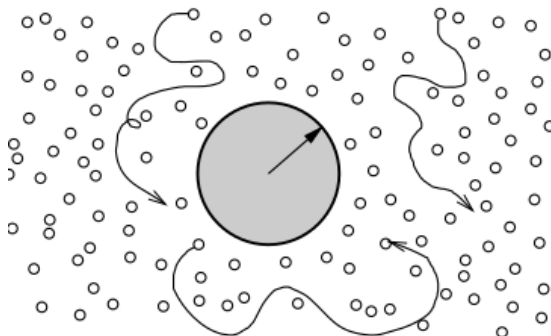


Figure 2.1: Schematic description of diffusing particles around an absorbing sphere [15]

the replenishment from the bulk of the gas molecules. In this context the case of interest is $d = 2$ for which this simplification do not hold since the diffusion is **recurrent**, but the rest of the calculation for $d = 3$ can be found in [15].

As said for $d = 2$ (and actually also for $d \leq 2$), the diffusion is recurrent, implying that during the absorption a continuously growing region of depletion develops around the object, eventually leading to a zero influx of particles for $t \rightarrow \infty$.

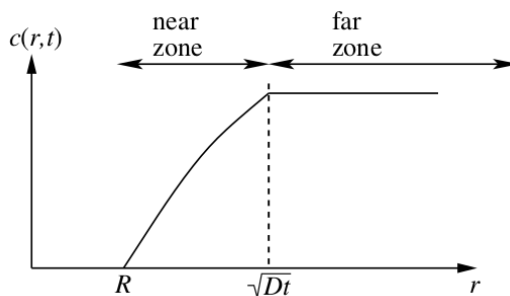


Figure 2.2: Sketch of density profile of quasi-static approximation, dividing space in “near” and “far” regions. [15]

To simplify this calculation a **quasi-static** approach is employed. The idea is that the region outside the absorbing object can be divided in a “near” region, within $r = \sqrt{Dt}$ and a complementary “far” region, see Fig.2.2. In the near region particles are affected by absorbing boundaries. Nevertheless a stationary state is assumed in this region, i.e it is assumed that the gas of particles reaches stationarity faster than the timescale of growth of the object, so that the concentration is nearly time independent. In the far region, instead, the probability of a particle of being absorbed is negligible because particles have a small probability to reach a distance

larger than \sqrt{Dt} in time t . Thus in the far zone the particle concentration remains $n(r) \simeq \bar{n}$.

Relying on this physical reasoning we can solve the Laplace equation in the near region, with the **time-dependent** boundary condition $n(r = \sqrt{Dt}) = \bar{n}$ to match the far region static solution.

The calculation from now on is carried out assuming that the object is a circle of radius R . The general solution of the Laplace equation for $d = 2$ is $n(r) = A + B \ln r$, so imposing the boundary conditions

$$n(r = \sqrt{Dt}) = \bar{n} \quad n(r = R) = n_0 \quad (2.2)$$

we obtain

$$n(r, t) = n_0 + \frac{\ln(r/R)}{\ln(\sqrt{Dt}/R)}(\bar{n} - n_0). \quad (2.3)$$

The reaction rate then can be found calculating the inward flux of particles, integrating over a circle of radius $r \gg R$ such that the diffusion coefficient of the molecules from the bulk of the gas can be used

$$K(t) = -D \int_{\Sigma} \nabla n \cdot \vec{r} d\Sigma = -D \int_0^{2\pi} d\theta \frac{\partial n}{\partial r} R \quad (2.4)$$

obtaining

$$K(t) = \frac{2\pi D(\bar{n} - n_0)}{\ln(\sqrt{Dt}/R)}. \quad (2.5)$$

2.2 Aggregation

Aggregation is a fundamental nonequilibrium process, in which reactive clusters join irreversibly when they meet. It underlies a large variety of phenomena, in this context the general framework is presented and then the more specific model of Island Growth is developed in Sec.(2.2.1).

The primary aggregation process may be represented as



two clusters of mass i and j join irreversibly at rate K_{ij} to form a cluster of mass $i+j$ (fig.2.3). Aggregation is manifestly irreversible, the number of clusters decrease with time, and eventually just one big cluster is left. The goal of this section is to write in a general way the equation governing the evolution of the concentration of clusters of mass k in time, $c_k(t)$.

We assume that the mass k runs over positive integers, i.e. that a cluster of mass k is formed by k minimal mass units. With this convention the reaction rates form

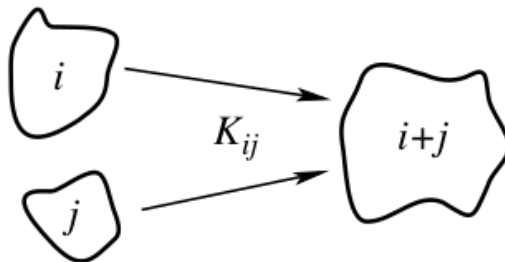


Figure 2.3: Irreversible merge of clusters of mass i and j . [15]

an infinite symmetric matrix $K_{i,j} = K_{j,i}$.

The starting point to treat aggregation is an infinite set of mean-field equations that approximately describe how the cluster mass distribution $c_k(t)$ evolves in time

$$\frac{dc_k}{dt} = \frac{1}{2} \sum_{i+j=k} K_{ij} c_i c_j - c_k \sum_{i \geq 1} K_{ki} c_i. \quad (2.7)$$

The first term in the r.h.s accounts for creation of clusters of mass k by the merging of two clusters of appropriated masses i and j . The factor $\frac{1}{2}$ is present due to double counting of different mass pairs, and correctly counts the same mass pairs of clusters. For a more accurate explanation of this see [15]. The second term instead is a loss term due to merging of a mass k cluster with any other, here the prefactor is correctly not present also for same mass pairs since two clusters disappear in a collision like $K_{jj} c_j c_j$. A more clear way to correctly account for this is

$$\frac{dc_k}{dt} = \frac{1}{2} \sum_{i,j \geq 1} K_{ij} c_i c_j (\delta_{i+j,k} - \delta_{i,k} - \delta_{j,k}) \quad (2.8)$$

This is the general equation governing aggregation phenomena that will be later applied. The underlying assumptions of this mean-field equation approach have to be kept in mind:

- **Cluster Locations:** Cluster positions are ignored, the assumption is that the system is well mixed s.t. the probability that multiple reactants are in proximity factorizes as a product of single particle densities. This amounts to a **mean-field** approximation.
- **Bimolecular reactions:** System is assumed to be dilute such that higher body interactions can be neglected.
- **Shape independence:** The cluster mass is the only relevant variable in the dynamics, shape plays no role

- Thermodynamic limit: The cluster masses are treated as continuous functions.

With this general framework now we can review the more specific case of the Island Growth model.

2.2.1 Island Growth Model

This model is an example of aggregation with input. Its two main features are:

- Particles are inserted onto the surface with rate F
- “Islands”, i.e. clusters with size larger or equal than 2 are immobile, only single monomers are mobile.

This implies that the islands can grow only by the addition of mobile monomers to their boundaries. For a schematic representation of this see fig 2.4

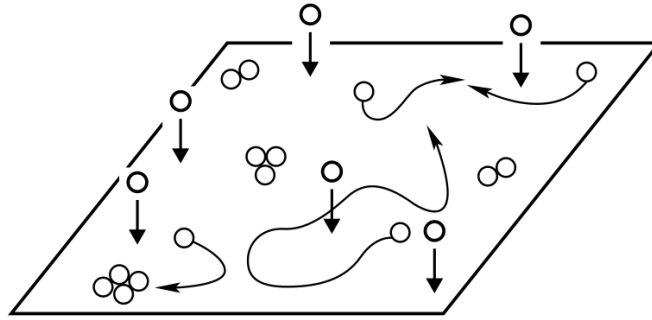
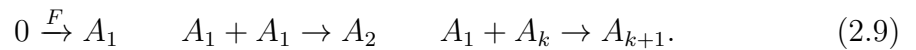


Figure 2.4: Illustration of fundamental processes in island growth model, adsorption at rate F , monomer collision to form a dimer, monomer aggregation to larger cluster. [15]

The elementary steps are:



The first process accounts for the deposition of particles onto the surface with rate F , the other two to cluster growth. Since only monomers can move, the reaction matrix simplifies to $K_{ij} \sim D_i + D_j = (\delta_{i,1} + \delta_{j,1})$, with D diffusivity of monomers. Inserting this into Eq.(2.8), distinguishing between the dynamics of the monomers and large clusters (which are different), and considering for monomers also the particle deposition rate we obtain

$$\begin{aligned} \frac{dc_1}{dt} &= -Dc_1 \sum_{k=1}^{\infty} c_k - Dc_1^2 + F \\ \frac{dc_k}{dt} &= Dc_1(c_{k-1} - c_k), \quad k \geq 2. \end{aligned} \quad (2.10)$$

The underlying assumptions are the ones of the general aggregation theory plus:

- Islands are so dilute that they can't merge directly;
- Islands are point like. This is actually a mild assumption since in the reaction rate in $d = 2$, Eq.(2.5) shows just a logarithmic dependence from the island radius;
- There are immobile islands and moving particles.

Now we are interested in computing the dynamics of the density of immobile islands $I = \sum_{k \geq 2} c_k$, for later use.

Summing over the second of Eqs.(2.10) we obtain:

$$\sum_{k=2}^{+\infty} \frac{dc_k}{dt} = Dc_1 \left(\sum_{k=2}^{+\infty} c_{k-1} - \sum_{k=2}^{+\infty} c_k \right) \quad (2.11)$$

which shifting the index of the first sum and recognizing the definition of I in the l.h.s gives

$$\frac{dI}{dt} = Dc_1^2. \quad (2.12)$$

This relation tells us that in this kind of model the number density of the domains larger than two monomers, the islands, is linearly proportional to the diffusion coefficient of the particles and quadratically to their density.

2.3 Phenomenological Theory

The model proposes two main ingredients to explain molecular sorting [3, 4]: (a) phase separation of specific molecules into localized sorting domains and (b) the introduction of a coupling between the molecule presence and the spontaneous curvature of the membrane, that after the domain reaches a sufficiently large radius leads to the formation of a vesicle.

In this picture molecules arrive onto the surface, diffuse and can then aggregate into localized enriched domains, which grow due to particle absorption. When the size of the domain is sufficiently big then the spontaneous curvature induced is enough to nucleate a vesicle, which is constitutively enriched in the biochemical components of the engulfed domains. This results into a spontaneous distillation process.

This process can be summarized as follows: molecules arrive onto the surface with a constant flux ϕ , diffuse, and can aggregate in localized enriched domains, which are then extracted when they reach a characteristic size R_E . The membrane coexists in a non-equilibrium statistically stationary state with the dilute, freely diffusing,

“gas” of molecules, which is continuously repleted. This process occurs through the typical stages of phase separation: after the initial nucleation stage, we consider to be in a “low supersaturation” context (this is correct if the average molecule density \bar{n} of the gas is sufficiently small), so the supercritical domain growth is driven by diffusion.

This is reminiscent of the Diffusion Limited Aggregation (DLA), in which at late time dynamics large fractal clusters form. In this context the presence of the cut-off radius R_E prevents this, and the domains remain approximately round.

Here, as in classical theories of nucleation [16], a critical radius R_C beyond which a cluster grows irreversibly is present.

The molecules gas density in the region just outside the domains n_0 is different from the bulk molecule density \bar{n} , due to the absorption which results in a depletion of the gas near the cluster. For clusters of size $R \gg R_C$ the density n_0 is independent from the domain size, (from the Gibbs-Thomson relation [4]). When the typical interdomain half distance L is much larger than the extraction radius R_E the difference between the bulk and near boundary density Δn is given approximately by $\Delta n \sim (\bar{n} - n_0) > 0$.

In the classical theories of nucleation, domains grow arbitrarily and Δn tends to zero. Here this is prevented from the presence of the extraction radius $R_E \gg R_C$, and the molecules density difference Δn is kept finite (and constant in a statistical sense?) by the continuous particle insertion onto the surface.

With this picture in mind we can study the quasi static density profile outside a supercritical cluster, employing the Reaction Rate theory presented in (2.1). The moving boundary considered before here reduces to a static one and its role is played by L , which now represents the limit of the area that can be influenced by a domain, due to presence of other domains. We obtain

$$n(r) = n_0 + \frac{\ln(r/R)}{\ln(L/R)}(\bar{n} - n_0), \quad (2.13)$$

with r distance from domain center and R size of the domain. Following the same reasoning we can calculate the inward flux of particles into the domain,

$$\Phi_R = -D \int_{\Sigma} \nabla n \cdot \vec{r} d\Sigma = -D \int_0^{2\pi} d\theta \frac{\partial n}{\partial r} R = \frac{2\pi D \Delta n}{\ln(L/R)}, \quad (2.14)$$

where D is the diffusion coefficient in the bulk of the gas. Alternatively the flux can be written highlighting the dependence from the area

$$\Phi_A = \frac{4\pi D \Delta n}{\ln(L^2/R^2)} = \frac{4\pi D \Delta n}{\ln(A_L/A)}, \quad (2.15)$$

with $A = \pi R^2$ area of a domain of radius R and $A_L = \pi L^2$ the area occupied by a circular region of radius L . The area variation of a cluster is caused by the inward

flux of particles, so we can write the dynamical equation for domain growth as

$$\dot{A} = \Phi_A A_0, \quad (2.16)$$

with A_0 the area occupied by a single diffusing particle. The equation can be rewritten as

$$\dot{A} = \frac{4\pi A_0 D \Delta n}{\ln(A_L/A)}. \quad (2.17)$$

Assuming that the sorting domains are approximately evenly distributed onto the membrane, the statistics of the supercritical domains can be described by the number density $N(A, t)dA$, which is the average number density of domains per unit of surface area with dimension between A and $A + dA$. The density satisfies the continuity equation

$$\frac{\partial N}{\partial t} + \frac{\partial(\dot{A}N)}{\partial A} = -\gamma(A)N, \quad (2.18)$$

with $\gamma(A)$ a parameter encoding in a mesoscopic way the rate of extraction of domains of size A , which assumes the values $\gamma(A) = 0$ for $A < A_E$ and $\gamma(A) = \gamma_0$ for $A > A_E$.

A stationary solution of (2.18) can be found solving directly the following separable differential equation

$$\frac{\dot{A}}{N_{st}} \frac{dN_{st}}{dA} = -\frac{\partial \dot{A}}{\partial A} - \gamma(A), \quad (2.19)$$

which, separating the variables and integrating between A_c and a generic A , gives

$$\ln \left(\frac{N_{st}(A)}{\text{const}} \right) = - \int_{A_c}^A \frac{1}{\dot{A}} \frac{d\dot{A}}{dA} dA - \int_{A_c}^A \frac{\gamma(A)}{\dot{A}} dA. \quad (2.20)$$

The integrand of the first term of the r.h.s can be rewritten as the derivative of the logarithm of \dot{A} , so it becomes

$$- \int_{A_c}^A \frac{d}{dA} (\ln \dot{A}) dA = - \ln \left(\frac{\dot{A}(A)}{\text{const}} \right), \quad (2.21)$$

taking $\dot{A}(A_c)$ as a constant. Finally inverting the logarithm and bringing all constants together (also A_0) into J we obtain

$$N_{st}(A) = \frac{J \ln(A_L/A)}{4\pi D \Delta n} \exp \left[- \int_{A_c}^A da \frac{\gamma(a) \ln(A_L/a)}{4\pi A_0 D \Delta n} \right]. \quad (2.22)$$

The normalization factor J can be found imposing that in the stationary regime the flux of incoming particles ϕ equals the average flux of particles being absorbed into the domains, i.e.

$$\phi = \int_{A_c}^{\infty} \Phi_A N_{st}(A) dA. \quad (2.23)$$

The integral can be divided in the interval between A_c and A_E and A_E to $+\infty$. In the second interval we assume γ_0 very large, i.e. we assume that the extraction factor strongly suppresses the number density. This gives a negligible contribution, leaving us with $\phi \simeq J(A_E - A_c) \simeq JA_E$, for $A_E \gg A_c$.

In the regime $A < A_E$ the number density has a universal logarithmic behaviour. Assuming that the incoming flux of particles ϕ is on average divided evenly among all the available supercritical domains, we can estimate the average number of supercritical domains per unit area as

$$\bar{N}_d \sim \frac{\phi}{\Phi_A} \sim \frac{\phi}{D\Delta n}, \quad (2.24)$$

neglecting logarithmic corrections.

The efficiency of the process can be characterized in terms of the average time of residence of a molecule onto the membrane system \bar{T} . From the moment of insertion particles spend an average time \bar{T}_f freely diffusing, and an average time \bar{T}_d inside a supercritical domain before extraction. In principle also the time spent in subcritical domains should be considered, but this is negligible if the critical size is small enough [4].

The freely diffusing time can be estimated as follows, clearly it is inversely proportional to the average number density of supercritical domains, and to the diffusion constant (with growing D also the root mean square distance \sqrt{Dt} grows, increasing the probability to encounter a domain), so

$$\bar{T}_f \sim \frac{1}{D\bar{N}_d} \sim \frac{\Delta n}{\phi}. \quad (2.25)$$

The time spent inside a domain instead can be estimated as the time in which flow of particles of flux Φ_A , each occupying an area A_0 , fill an area A_E , so

$$\bar{T}_d \sim \frac{A_E}{A_0\Phi_A} \sim \frac{A_E}{A_0D\Delta n}, \quad (2.26)$$

neglecting logarithmic corrections. The rate of formation of new domains can be estimated employing Eq.(2.12), since the present situation fits into the framework of Island growth model (the part of the process concerning the aggregation of particles into domains). A dimensionless constant is introduced here that accounts for the efficiency of absorption of single molecules by germs of domains, obtaining

$$\frac{dN_d}{dt} = CD\bar{n}^2. \quad (2.27)$$

In a stationary state this is also given by $dN_d/dt = N_d/\bar{T}_d$, allowing to estimate the scaling of \bar{n} as

$$\bar{n} \sim \left(\frac{\phi A_0}{CDA_E} \right)^{1/2}. \quad (2.28)$$

Assuming $\bar{n} \gg n_0$ (i.e that the domains absorb rapidly, such that the depleted region near the domains has a very low density), and thus $\Delta n \sim \bar{n}$ we obtain

$$\hat{T}_f \sim \frac{\bar{n}}{\phi} \sim C^{-1/2} \left(\frac{A_0}{DA_E\phi} \right)^{1/2} \quad (2.29)$$

and

$$\hat{T}_d \sim \frac{A_E}{DA_0\bar{n}} \sim C^{1/2} \left(\frac{A_E}{A_0} \right)^{3/2} (D\phi)^{-1/2}. \quad (2.30)$$

The total residence time $\bar{T} = \bar{T}_f + \bar{T}_d$ has minimum w.r.t C , in $C \sim (A_0/A_E)^2$. At the minimum

$$\bar{T}_f \sim \bar{T}_d \sim \left(\frac{A_E}{A_0} \right)^{1/2} (D\phi)^{-1/2} \quad (2.31)$$

and

$$\bar{n} \sim \left(\frac{\phi A_E}{DA_0} \right)^{1/2}. \quad (2.32)$$

These two scaling relations identify the optimal dynamical regime, in which molecular sorting is most efficient. The density of particles inside the domains can also be estimated from

$$\rho_d \sim N_d \frac{A_E}{A_0} \sim C^{1/2} \left(\frac{\phi}{D} \right)^{1/2} \left(\frac{A_E}{A_0} \right)^{3/2} \quad (2.33)$$

that is the number of domains per unit area multiplied for the number of particles inside a domain. Repeating the calculation for the minimum w.r.t C for the total density $\rho = \hat{n} + \rho_d$ we find the same minimum $C \sim (A_0/A_E)^2$, and the density ρ evaluated in such minimum gives the same result as Eq.(2.32).

2.4 Lattice gas Model

To further explore the distillation process a minimal lattice gas model of molecule sorting is introduced. The membrane is described as a two dimensional square lattice with periodic boundary conditions, where each site can host only one molecule. The system evolves as a Markov process characterized from the three following moves:

- Molecules from an infinite reservoir arrive onto the surface and are inserted in empty sites with rate k_I .
- Then molecules can perform diffusive jumps to any empty neighbour with rate $k_D/g^{N_{nn}}$, with k_D diffusion rate, g dimensionless coefficient accounting for the particles tendency to stick together when they meet, and N_{nn} the number of occupied neighbors of the site originally occupied by the jumping particle.

- Finally, particles are extracted removing all the connected components, if present, which occupy completely a square area of linear size R_E^2/A_0 .

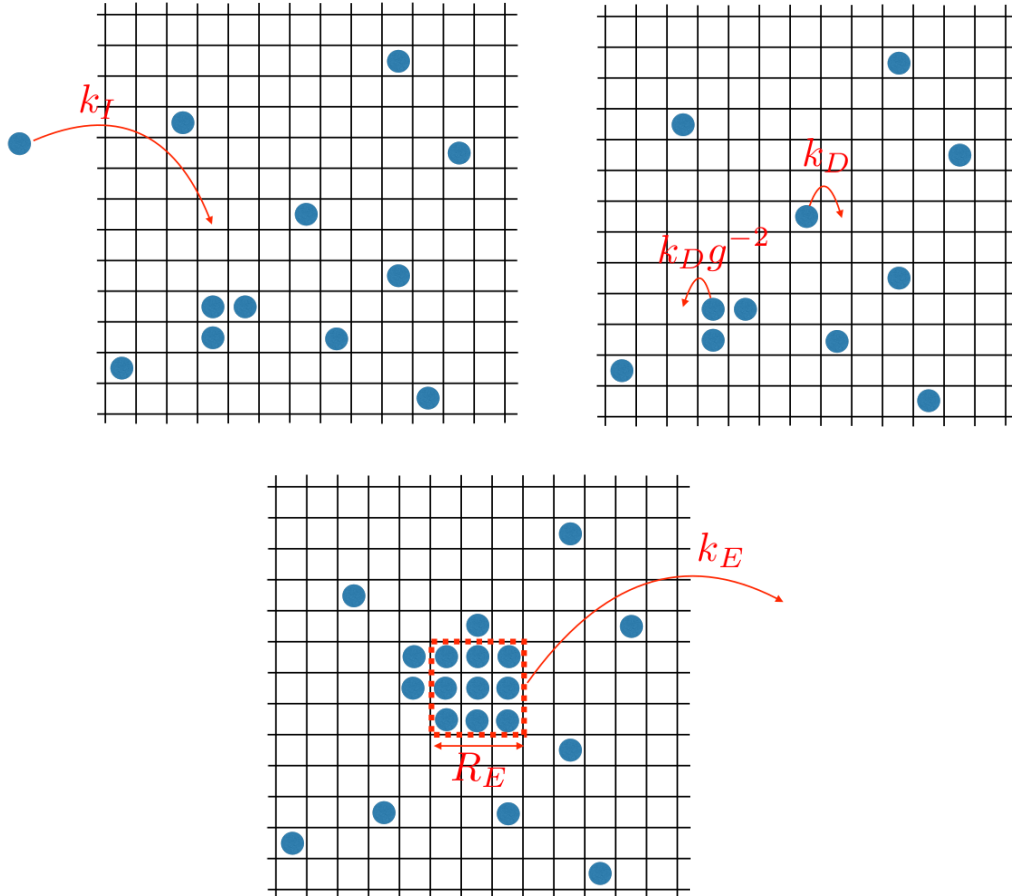


Figure 2.5: The three possible moves of the Markov process: On the upper left particle insertion, on the upper right particle diffusion, below cluster extraction.

Chapter 3

Field-Theoretic Description of a Fluid Membrane

Since the goal of this work is to extend the model presented in the previous chapter onto a fluctuating membrane, in this chapter the framework in which the membrane is studied (and simulated) is presented. As it's known surfaces in dimension greater than one are influenced from fluctuations at any nonzero temperature, and thus are not microscopically flat [17].

The nature of this fluctuations depend from the energy of the different non-flat configurations. In the following, first some useful tools from differential geometry that allows one to describe this kind of configurations will be reviewed; then the different energy contributions that can be considered will be discussed, presenting the Helfrich hamiltonian. Finally, the fluctuations of the model will be analyzed, and the concept of crumpling transition will be reviewed.

This kind of reasoning treats the membrane as a two dimensional surface with zero thickness. This is justified in the limit in which the lateral extent of the membrane is large compared to its thickness, but this is true in typical problems in membrane biophysics in which a mesoscale approach is employed [10]. The model employed in this work is of a fluid membrane, i.e. a membrane composed of molecules that can freely diffuse onto the plane, and that cannot support a shear stress.

3.1 Differential geometry and total surface area

A surface S is a $(d - 1)$ -dimensional manifold embedded in a d -dimensional space. Points on the surface can be specified by a d -dimensional vector $\vec{R}(\vec{u})$, function of the $(d - 1)$ coordinates $\vec{u} = (u^1, \dots, u^{d-1})$. Any set of $d - 1$ independent coordinates can be used to parameterize the surface, so suitable choices are made for particular geometries. In this context we are interested to describe quasi-flat configurations

so we will focus on the **Monge** gauge. In this gauge the radius is the following functional

$$\vec{R}(\vec{x}_\perp) = (\vec{x}_\perp, h(\vec{x}_\perp)), \quad (3.1)$$

with $\vec{x}_\perp = (x_1, x_2, \dots, x_{d-1})$ coordinates in a fixed plane in space, and $h(\vec{x}_\perp)$ a function that specifies the height of the surface above such base plane. In general the surface can have overhangs, for which case the Monge gauge might not be the best choice since the function $h(\vec{x}_\perp)$ would be a multi valued function. In some cases it would be possible to avoid this problem rotating the base plane, such that w.r.t the new base plane the surface has no overhangs, as shown in (3.1).

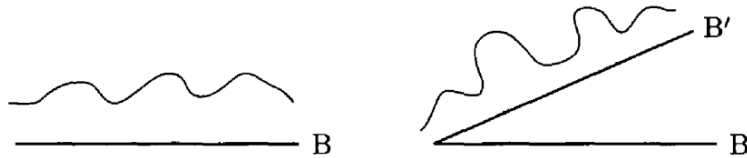


Figure 3.1: On the left surface with no overhangs, on the right surface that w.r.t the base plane B has overhangs but not w.r.t the rotated base plane B' . [17]

An equivalent formulation of the Monge gauge is to specify the height of the surface above the base plane through the zeros of the function

$$\psi(\vec{x}) = x_d - h(\vec{x}_\perp) \quad (3.2)$$

where $\vec{x} = (\vec{x}_\perp, x_d)$ is a d -dimensional vector.

To simplify in the following we focus on the case of surfaces of two and three dimensions, in the case of no overhangs. A one dimensional surface is simply a planar curve, which can be parameterized by a single scalar variable u . This means that

$$\vec{t} = \frac{d\vec{R}}{du} \quad (3.3)$$

is the tangent vector, and the length of the line segment between u and $u + du$ is $ds = (d\vec{R} \cdot d\vec{R})^{1/2}$. In the Monge gauge $\vec{R}(x) = (x, h(x))$, and

$$d\vec{R} = \left(\hat{e}_x, \frac{dh}{dx} \hat{e}_y \right) dx \quad (3.4)$$

with \hat{e}_x and \hat{e}_y versors of the x and y axes. The total length of the curve in the Monge gauge is then

$$L = \int_0^L ds = \int_0^{L_B} \left[1 + \left(\frac{dh}{dx} \right)^2 \right]^{1/2} dx, \quad (3.5)$$

where L_B is the length of the horizontal base line.

A two dimensional surface instead can be parameterized with two variables u^1, u^2 . The infinitesimal displacement along the surface is given by

$$d\vec{R} = \frac{\partial \vec{R}}{\partial u^1} du^1 + \frac{\partial \vec{R}}{\partial u^2} du^2, \quad (3.6)$$

with $\vec{t}_1 = \frac{\partial \vec{R}}{\partial u^1}$ and $\vec{t}_2 = \frac{\partial \vec{R}}{\partial u^2}$ the tangent vectors to the surface at (u^1, u^2) (not necessarily orthogonal). The infinitesimal surface element, the area of the parallelogram of sides du^1 and du^2 , is then

$$dS = \left| \frac{\partial \vec{R}}{\partial u^1} \times \frac{\partial \vec{R}}{\partial u^2} \right| du^1 du^2. \quad (3.7)$$

We can calculate this quantity in the Monge gauge, where we have $R(x_1, x_2) = (x_1, x_2, h(x_1, x_2))$, and we obtain

$$dS = \sqrt{1 + (\nabla_{\perp} h)^2} dx_1 dx_2, \quad (3.8)$$

where

$$\nabla_{\perp} h = \frac{\partial h}{\partial x_1} \hat{e}_{x_1} + \frac{\partial h}{\partial x_2} \hat{e}_{x_2}. \quad (3.9)$$

Then the total area of a surface with no overhangs and related to a fixed base plane is

$$A = \int dS = \int_{A_B} \sqrt{1 + (\nabla_{\perp} h)^2} dx_1 dx_2. \quad (3.10)$$

A normal can be constructed at each point of the surface, in three dimensions this is given by

$$\hat{N} = \frac{\vec{t}_1 \times \vec{t}_2}{|\vec{t}_1 \times \vec{t}_2|}. \quad (3.11)$$

The sign of the normal is not uniquely determined. It can be arbitrary if the two sides of the surface are indistinguishable, if not (for example the surface separates two different phases) a consistent convention has to be chosen. The plane normal to \hat{N} at P defines the tangent plane of the surface at P . An explicit form of the normal in the Monge gauge can be calculated from the result used also to calculate the surface area element

$$\vec{t}_1 \times \vec{t}_2 = \frac{\partial \vec{R}}{\partial x_1} \times \frac{\partial \vec{R}}{\partial x_2} = (-\nabla_{\perp} h, 1), \quad (3.12)$$

which gives

$$\hat{N} = \frac{1}{\sqrt{1 + (\nabla_{\perp} h)^2}} (-\nabla_{\perp} h, 1). \quad (3.13)$$

3.2 Curvature

On each point of a surface a curvature can be defined. For a planar curve the curvature is a scalar quantity, the inverse of the radius of the circle that follows locally the curve at P , see Fig.(3.2).

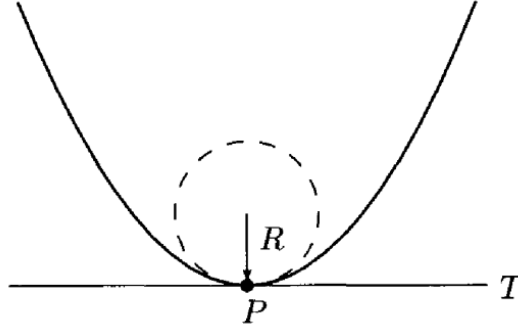


Figure 3.2: Planar curve, with T tangent plane at point P , and tangent circle of radius inverse of the curvature. [17]

Let's call T the tangent plane at P , x a coordinate along T with the origin in P , and $h(x) = \hat{N} \cdot \vec{R}$ the height of the curve above P with \vec{R} the radius defining the curve. For small x the height $h(x)$ can be expanded in power series around zero. Since T is the tangent at P $h(x)$ has a minimum in $x = 0$, so $dh(x)/dx|_{x=0} = 0$, implying

$$h(x) = K \frac{x^2}{2}. \quad (3.14)$$

Alternatively, as showed in Fig.(3.2), let's use the circle of radius R tangent at P . If the circle of the radius is along the normal \hat{N} , the curve height around P w.r.t the normal \hat{N} is $h' = R(1 - \cos \theta)$, with θ the angle measured from \hat{N} . Then if the angle $\theta = x/R$ is small, a second-order expansion gives

$$h'(x) = R^{-1} \frac{x^2}{2}, \quad (3.15)$$

so the circle and the curve match up to order x^2 if $K = R^{-1}$. If instead the center of the circle lies along $-\hat{N}$ we obtain $h' = -R(1 - \cos \theta)$ and $K = -R^{-1}$. So the curvature K has a positive sign if the curve rises towards \hat{N} and a negative one if it falls away from it. This is consistent with K being the second derivative of h evaluated in $x = 0$.

A similar reasoning can be carried out for a two dimensional surface S embedded in a three dimensional space. Let T be the tangent plane at a point P of S . Planes normal to T at P are called normal planes, each one intersecting the surface in a

planar curve called normal section. Being planar curves each normal section has an associated curvature. Let's define as x_1 and x_2 the basis vectors of an orthogonal coordinate system onto the tangent plane, with the origin in P . The height of the surface $h = \hat{N} \cdot \vec{R}$ above P can then be expanded in a power series in $x_\perp = (x_1, x_2)$, up to second order as before

$$h(\vec{x}_\perp) = \frac{1}{2} \sum_{i,j} K_{ij} x_i x_j, \quad (3.16)$$

where K is a 2x2 real symmetric matrix (the Hessian of the function $h(\vec{x}_\perp)$). Being real and symmetric K has two real eigenvalues R_1^{-1} , R_2^{-1} with associated orthonormal eigenvectors \hat{e}_1 , \hat{e}_2 . The eigenvectors form a base of T so

$$\vec{x}_\perp = \lambda_1 \hat{e}_1 + \lambda_2 \hat{e}_2, \quad (3.17)$$

which inserted into Eq.(3.16) gives:

$$h(\vec{x}_\perp) = \frac{1}{2} R_1^{-1} (\vec{x}_\perp \cdot \hat{e}_1)^2 + \frac{1}{2} R_2^{-1} (\vec{x}_\perp \cdot \hat{e}_2)^2. \quad (3.18)$$

R_1 and R_2 are called the principal radii of curvature of the surface at P and correspond to the radii of the circles that best fit the surface in the planes in which \hat{N} , \hat{e}_1 and \hat{N} , \hat{e}_2 respectively lie. The signs of R_1 and R_2 can either be positive or negative. If they are both positive (negative) all normal sections are directed towards (away from) the normal. If they have a different sign the point P identifies a saddle, as can be seen in Fig.(3.3).

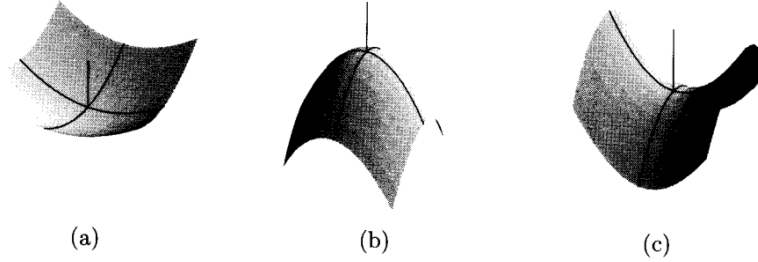


Figure 3.3: (a) surface with both positive principal curvature radii, (b) surface with both negative principal curvature radii, (c) surface with one positive one negative principal curvature radii.[17]

The curvature of the normal section containing the generic vector of T $\vec{e}(\gamma) = |\vec{e}(\gamma)|(\cos(\gamma)\hat{e}_1 + \sin(\gamma)\hat{e}_2)$ can be found inserting it into Eq.(3.18), obtaining

$$R^{-1}(\gamma) = R_1^{-1} \cos^2(\gamma) + R_2^{-1} \sin^2(\gamma). \quad (3.19)$$

The extremal values of $R^{-1}(\gamma)$ occur for $\gamma = 0 + a\pi$ and $\gamma = \frac{\pi}{2} + a\pi$ with a any integer, where $R^{-1}(\gamma)$ equals R_1^{-1} and R_2^{-1} respectively. This implies that the principal curvatures R_1 and R_2 correspond to the maximum and minimum curvatures of all the normal sections passing at P .

Two scalar invariants can be constructed from K , i.e.

$$\text{Tr } K = R_1^{-1} + R_2^{-1} = 2H_c, \quad (3.20)$$

$$\det K = \frac{1}{R_1 R_2} = H_G. \quad (3.21)$$

H_c is the mean curvature and H_G is the Gaussian curvature. The mean curvature in the Monge gauge can be approximated easily taking as a base plane the tangent plane at P . In this case to linear order in \vec{x}_\perp we obtain

$$\hat{N} = (-\nabla_\perp h, 1) = \left(-\sum_j K_{1j} x_j, -\sum_j K_{2j} x_j, 1\right), \quad (3.22)$$

implying $\nabla_\perp \cdot \hat{N} = -\text{Tr } K$. Then

$$\frac{1}{R_1} + \frac{1}{R_2} = -\nabla_\perp \cdot \hat{N} = -\frac{\nabla_\perp^2 h}{[1 + (\nabla_\perp h)^2]^{3/2}}. \quad (3.23)$$

3.3 Continuous Model of a fluid membrane

It is widely known in the literature [6, 7, 8] that the behaviour of a thin (with thickness small compared to scales describing its shape) fluid (formed by constituents that can freely diffuse) membrane can be described with a continuum model based on the following Hamiltonian

$$\mathcal{H}_{el} = \int dS \left[\frac{k}{2} (H_c - H_0)^2 + \bar{k} H_G \right] \quad (3.24)$$

which is known as Helfrich Hamiltonian. This functional considers only elastic energy terms, in more general cases of fluctuating surfaces also other energy contributions can be considered, such as surface tension, but here they will be neglected. This is justified by the fact that actual fluid membranes often have very small or negligible surface tension [18], and the absence of such energy term actually determines the strong fluctuations characteristic of this systems. This is a purely geometrical model, considering as energy contributions the deviations from flatness, quantified by the mean curvature H_c and the Gaussian curvature H_G . The mean curvature term measures the deviation from $H_0 = 2/R_0$, a local spontaneous curvature. If for example the lowest energy state is the flat configuration then $R_0 = \infty$.

The Gaussian curvature contribution instead, according to the **Gauss-Bonnet** theorem, it's constant on surfaces of fixed topology. This implies that this term does not influence fluctuations of surfaces of constant topology.

Now we want to calculate the Hamiltonian in the Monge gauge. If we consider a surface that has a fixed topology, we can neglect the Gaussian curvature. Furthermore, if the surface is quasi-flat, we can perform the harmonic approximation, i.e. keeping the field h only up to the second order,

$$\mathcal{H}_{har}[h] = \frac{1}{2}k \int d\vec{x}_\perp (\nabla^2 h)^2. \quad (3.25)$$

In order to study the fluctuations we write the Hamiltonian in Fourier space

$$\mathcal{H}_{har}[\hat{h}] = \frac{1}{2}k \int \frac{d\vec{q}}{(2\pi)^{d-1}} q^4 |\hat{h}(\vec{q})|^2. \quad (3.26)$$

We recall that when the partition function is a Gaussian functional integral (i.e. the action is quadratic) the following result for the two point correlation function holds

$$\langle \hat{h}(\vec{q}) \hat{h}(\vec{q}') \rangle = (2\pi)^{(d-1)} \delta(\vec{q} + \vec{q}') \hat{G}(\vec{q}), \quad (3.27)$$

where $\hat{G}(\vec{q})$ is the Gaussian propagator in Fourier space, which in this case is just a scalar $\hat{G}(\vec{q}) = \frac{k_B T}{k q^4}$. So we obtain the real space two point correlation function

$$\begin{aligned} \langle h^2(\vec{x}_\perp) \rangle &= \int \frac{d\vec{q} d\vec{q}'}{(2\pi)^{2(d-1)}} \langle \hat{h}(\vec{q}) \hat{h}(\vec{q}') \rangle e^{i\vec{x}_\perp \cdot (\vec{q} + \vec{q}')} \\ &= \int_{1/L_B}^\Lambda \frac{d\vec{q}}{(2\pi)^{(d-1)}} \frac{k_B T}{k q^4} \end{aligned} \quad (3.28)$$

where L_B is the largest length scale of the system (corresponding to the smallest wavevector), and Λ is an upper cut off momentum, that will be set to $1/a$, where a is the smallest unit of length of the system. Specifying the dimension we obtain

$$\langle h^2(\vec{x}_\perp) \rangle = \int_{1/L_B}^{1/a} \frac{d^2 q}{(2\pi)^2} \frac{k_B T}{k q^4} = \frac{k_B T (L_B^2 - a^2)}{6\pi k} \simeq \frac{k_B T L_B^2}{6\pi k}, \quad d = 3 \quad (3.29)$$

since $L_B \gg a$. Thus a two dimensional surface embedded in three dimensions has height fluctuations that diverge with the size of the surface. The average position of such a surface becomes less well defined as the surface dimension increases, that means that the surface lacks **long-range positional order**. It is interesting to compute the fluctuations also for the direction of the surface normal.

Since we are considering quasi-flat configurations the average direction of the surface can be taken as $\hat{e} = (0,0,1)$. Then the surface normal deviations from the average normal can be written as

$$\delta \hat{N}(\vec{x}_\perp) \approx \hat{N}(\vec{x}_\perp) - \hat{e} \approx (-\nabla_\perp h), \quad (3.30)$$

using Eq.(3.23), and we can write for the fluctuations

$$\langle |\delta \hat{N}(\vec{x}_\perp)|^2 \rangle \approx \langle (\nabla_\perp^2 h)^2 \rangle = \langle h^2(\vec{x}_\perp) \rangle = - \int \frac{d\vec{q} d\vec{q}'}{(2\pi)^{2(d-1)}} \vec{q} \cdot \vec{q}' \langle \hat{h}(\vec{q}) \hat{h}(\vec{q}') \rangle e^{i\vec{x}_\perp \cdot (\vec{q} + \vec{q}')}, \quad (3.31)$$

where the minus factor in front comes from the imaginary units coming down from the orthogonal gradient of the exponentials. Then substituting Eq.(3.27) and integrating the Dirac delta

$$\begin{aligned} \langle |\delta \hat{N}(\vec{x}_\perp)|^2 \rangle &\approx \int \frac{d\vec{q}}{(2\pi)^{(d-1)}} \frac{k_B T q^2}{k q^4} \\ &\approx \int_{1/L_B}^{1/a} \frac{d^2 q}{(2\pi)^2} \frac{k_B T}{k q^2} = \frac{k_B T}{2\pi k} \ln(L_B/a). \quad d = 3 \end{aligned} \quad (3.32)$$

This implies that also fluctuations of the normal diverge with the system dimension, and thus also **long-range orientational order** is not present.

From this result also a persistence length pertaining the orientational order can be computed, defined as the length scale at which the normal fluctuations become of order unity, obtaining

$$\xi_p = a e^{\frac{2\pi k}{k_B T}}. \quad (3.33)$$

which is called the De Gennes-Taupin persistence length [19]. This implies that for length scales larger than ξ_p orientational order is lost, and the surface becomes **crumpled**, as it's shown in Fig(3.4). The fact that the persistence length is always finite for any nonzero temperature means that fluid membranes described from Hamiltonians of the type of Eq.(3.24) for large enough length scales are always crumpled [7].

This result can be obtained more formally employing renormalization techniques [20], as it will be reviewed in the next section.

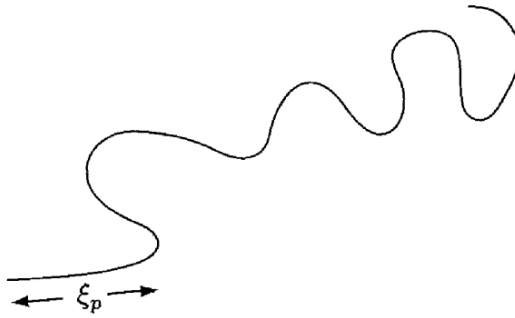


Figure 3.4: Representation of crumpling at lengthscales larger than ξ_p [17].

3.4 The Crumpling transition

To explore how short-ranged fluctuations renormalize the bending rigidity (and thus see if a repulsive fixed point is found in the flow equation at nonzero temperature, signaling a phase transition between a flat and a crumpled phase) we employ Wilson's momentum shell renormalization group approach [21]. With this tool we can lift the harmonic approximation¹ and study the mean curvature energy considering also higher order terms as

$$\begin{aligned}\mathcal{H}_{el}[h] &= \frac{1}{2}k \int d^2x_{\perp} [(\nabla_{\perp}^2 h)^2 [1 + (\nabla_{\perp} h)^2]^{-5/2}], \\ &\approx \int d^2x_{\perp} \left[\frac{k}{2} (\nabla_{\perp}^2 h)^2 - \frac{\alpha}{2} k (\nabla_{\perp} h)^2 (\nabla_{\perp}^2 h)^2 \right].\end{aligned}\quad (3.34)$$

The prefactor of the fourth order term is kept as a parameter α . The calculation will be carried out in a generic dimension d , and restricted to case of interest $d = 2$ at the end (here d is referred to the surface dimension, with $d + 1$ the dimension of the space in which it is embedded). We take the Fourier transform of the height field

$$h(\vec{x}_{\perp}) = \int \frac{d^d q}{(2\pi)^d} \hat{h}(\vec{q}) e^{i\vec{q} \cdot \vec{x}_{\perp}}, \quad (3.35)$$

and find the functional in momentum space

$$\begin{aligned}\mathcal{H}_{el}[\hat{h}] &= \int \frac{d^d q}{(2\pi)^d} \frac{kq^4}{2} |\hat{h}(\vec{q})|^2 - \frac{\alpha}{2} k \int \frac{d^d q_1 d^d q_2 d^d q_3}{(2\pi)^{3d}} \hat{h}(\vec{q}_1) \hat{h}(\vec{q}_2) \hat{h}(\vec{q}_3) \times \\ &\times \hat{h}(-\vec{q}_1 - \vec{q}_2 - \vec{q}_3) (q_1^2 q_2^2 (\vec{q}_3 \cdot (\vec{q}_1 + \vec{q}_2 + \vec{q}_3))).\end{aligned}\quad (3.36)$$

The field is divided in fast and slow modes as $\hat{h}(\vec{q}) = \hat{h}_{<}(\vec{q}) + \hat{h}_{>}(\vec{q})$, with the slow modes involving momenta in the range $0 < \vec{q} < \Lambda/l$. To renormalize the Hamiltonian we will integrate over fast modes, that are nonzero in the momentum shell $\Lambda/l < \vec{q} < \Lambda$. The Gaussian term and the interaction term that couples fast and slow modes are identified respectively as

$$\begin{aligned}\mathcal{H}_0 &= \int \frac{d^d q}{(2\pi)^d} \frac{kq^4}{2} |\hat{h}(\vec{q})|^2, \\ \mathcal{H}_I &= -\frac{\alpha}{2} k \int \frac{d^d q_1 d^d q_2 d^d q_3}{(2\pi)^{3d}} \hat{h}(\vec{q}_1) \hat{h}(\vec{q}_2) \hat{h}(\vec{q}_3) \hat{h}(-\vec{q}_1 - \vec{q}_2 - \vec{q}_3) (q_1^2 q_2^2 (\vec{q}_3 \cdot (\vec{q}_1 + \vec{q}_2 + \vec{q}_3))).\end{aligned}\quad (3.37)$$

¹This is actually necessary to investigate how thermal fluctuations renormalize the bending rigidity, in a quadratic Hamiltonian different wavelength modes fluctuate independently [22].

The renormalized action is given by the expansion

$$\mathcal{H}'_{el}[h_{<}] = \mathcal{H}_0[h_{<}] + \langle \mathcal{H}_I \rangle_{0,>} - \frac{\beta}{2} (\langle \mathcal{H}_I^2 \rangle_{0,>} - \langle \mathcal{H}_I \rangle_{0,>}^2) + \dots, \quad (3.38)$$

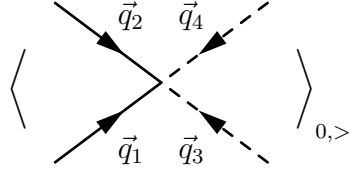
where the notation $\langle \cdot \rangle_{0,>}$ identify the average over the Gaussian measure related to fast modes,

$$\langle A \rangle_{0,>} = \frac{\int Dh_{>} A e^{-\beta \mathcal{H}_0[h_{>}]}}{Z_{0,>}}. \quad (3.39)$$

With this framework we calculate the one loop correction to the bending rigidity. The first order corrections are given by

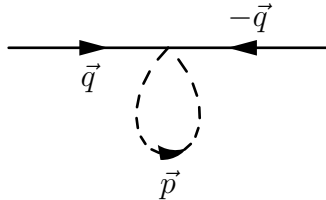
$$\langle \mathcal{H}_I \rangle_{0,>} = -\frac{\alpha}{2} k \int \frac{d^d q_1 d^d q_2 d^d q_3 d^d q_4}{(2\pi)^{4d}} \langle \hat{h}(\vec{q}_1) \hat{h}(\vec{q}_2) \hat{h}(\vec{q}_3) \hat{h}(\vec{q}_4) \rangle_{0,>} \delta\left(\sum_{i=1}^4 \vec{q}_i\right) q_1^2 q_2^2 (-\vec{q}_3 \cdot \vec{q}_4). \quad (3.40)$$

We evaluate such terms using Wick's theorem in a diagrammatic representation. The only term that has the correct dependence from the wavevector \vec{q} to renormalize k is given by the following contribution



$$\langle \text{Diagram} \rangle_{0,>}, \quad (3.41)$$

In which the two slow modes are the ones related to the terms that contained the Laplacian, that have a quadratic contribution in the momentum. This gives a correction proportional to the fourth power of the momentum, which renormalizes the bending rigidity. The correction is



$$= \int^{\Lambda/l} \frac{d^d q}{(2\pi)^d} q^4 |\hat{h}_{<}(\vec{q})|^2 \int_{\Lambda/l}^{\Lambda} \frac{d^d p}{(2\pi)^d} \frac{p^2 k_B T}{k^4}, \quad (3.42)$$

evaluating the fast mode two point correlation function, and inserting the expression of the Gaussian propagator. Inserting this correction the coarse-grained slow modes

action assumes the form

$$\begin{aligned} \mathcal{H}'_{el}[\hat{h}_<] &= \int^{\Lambda/l} \frac{d^d q}{(2\pi)^d} |\hat{h}_<(\vec{q})|^2 \frac{k_1 q^4}{2} - \frac{\alpha}{2} k \int^{\Lambda/l} \frac{d^d q_1 d^d q_2 d^d q_3}{(2\pi)^{3d}} \hat{h}_<(\vec{q}_1) \hat{h}_<(\vec{q}_2) \hat{h}_<(\vec{q}_2) \times \\ &\times \hat{h}_<(-\vec{q}_1 - \vec{q}_2 - \vec{q}_3) q_1^2 q_2^2 (\vec{q}_3 \cdot (\vec{q}_1 + \vec{q}_2 + \vec{q}_3)), \end{aligned} \quad (3.43)$$

considering also the first order correction with all slow modes arising from Eq.(3.40), and with the corrected bending energy

$$k_1 = k \left[1 - \alpha \int_{\Lambda/l}^{\Lambda} \frac{d^d p}{(2\pi)^d} \frac{k_B T}{k p^2} \right]. \quad (3.44)$$

Then introducing momentum rescaling $\vec{q}' = \vec{q}l$ and field renormalization $\hat{h}(\vec{q}) = \hat{h}'(\vec{q}')z$, the renormalized effective action is

$$\begin{aligned} \mathcal{H}'_{el}[\hat{h}'] &= \int^{\Lambda} \frac{d^d q'}{(2\pi)^d} l^{-d} \frac{k_1 (q')^4}{2} l^{-4} |\hat{h}'(\vec{q}')|^2 z^2 - \frac{\alpha}{2} k \int^{\Lambda} \frac{d^d q'_1 d^d q'_2 d^d q'_3}{(2\pi)^{3d}} l^{-3d} \hat{h}'(\vec{q}'_1) \hat{h}'(\vec{q}'_2) \times \\ &\times \hat{h}'(\vec{q}'_3) \hat{h}'(-\vec{q}'_1 - \vec{q}'_2 - \vec{q}'_3) z^4 ((q'_1)^2 (q'_2)^2 (\vec{q}'_3 \cdot (\vec{q}'_1 + \vec{q}'_2 + \vec{q}'_3))) l^{-6}. \end{aligned} \quad (3.45)$$

The field renormalization z can be fixated imposing that the two bending rigidities have the same scaling, obtaining

$$z = l^{d+1} \quad (3.46)$$

which gives for the bending energy renormalized by the first order correction the following scaling

$$k' = k_1 l^{d-2}. \quad (3.47)$$

From now on the calculation is restricted to the case $d = 2$. The momentum shell integral can be evaluated exactly as

$$\int_{\Lambda/l}^{\Lambda} \frac{d^2 p}{(2\pi)^2} \frac{k_B T}{k p^2} = \frac{k_B T}{2\pi k} \ln(l), \quad (3.48)$$

giving the renormalization of k (at first order)

$$k(l) = k \left[1 - \frac{\alpha k_B T}{2\pi k} \ln(l) \right]. \quad (3.49)$$

The differential version of which can be written as following. Writing the spatial rescaling factor as $l = e^s$, for an infinitesimal δs

$$k + \frac{dk}{ds} \delta s + O(\delta s^2) = k \left[1 - \alpha \frac{k_B T}{2\pi k} \delta s + O(\delta s^2) \right], \quad (3.50)$$

which gives the flow equation

$$\frac{dk}{ds} = -\frac{\alpha k_B T}{2\pi}. \quad (3.51)$$

The absence of a fixed point confirms, as said previously, that fluid membranes in two dimensions are always crumpled. The prefactor α in [18], is determined to be $\alpha = \frac{3}{2}$.

3.5 Curvature Instability

A simple equilibrium model of particles coupled to the curvature and diffusing onto a fluid membrane [23, 24] is reviewed in this section. Defining the scalar density field of the particles as $\Phi(\vec{x}_\perp)$, the interaction term that couples the diffusing molecules with the surface spontaneous curvature is introduced as an energy term

$$\mathcal{H}_{int} = - \int dS \mu \Phi H_c. \quad (3.52)$$

Besides interacting with the surface the diffusing molecules interact also between themselves, so their energy contribution can be written as

$$\mathcal{H}_{part} = \int dS \left[\frac{1}{2} b |\nabla \Phi|^2 + \frac{1}{2} a \Phi^2 \right], \quad (3.53)$$

assuming as a simplification that the particle energy is Gaussian. More complicated energy terms describing the particles onto the surface could be considered, but already with this very simple treatment some conclusions can be drawn.

Then, still assuming that the surface has no spontaneous curvature itself and that it is topologically invariant, the total surface energy is

$$\mathcal{H}_{sur} = \int dS \left[\frac{1}{2} k H_c^2 - \mu \Phi H_c + \frac{1}{2} b |\nabla \Phi|^2 + \frac{1}{2} a \Phi^2 \right]. \quad (3.54)$$

This can be written in the Monge gauge writing the mean curvature using Eq.(3.23), and taking again the harmonic approximation in the height field, obtaining

$$\mathcal{H}_{sur}[h, \Phi] = \int d\vec{x}_\perp \left[\frac{1}{2} k (\nabla_\perp^2 h)^2 - \mu \Phi \nabla_\perp^2 h + \frac{1}{2} b |\nabla \Phi|^2 + \frac{1}{2} a \Phi^2 \right], \quad (3.55)$$

or in Fourier space

$$\mathcal{H}_{sur}[\hat{h}, \hat{\Phi}] = \int \frac{d\vec{q}}{(2\pi)^d} \left[\frac{1}{2} k q^4 |\hat{h}(\vec{q})|^2 + \mu q^2 \hat{\Phi}(\vec{q}) \hat{h}(-\vec{q}) + \frac{1}{2} (a + b q^2) |\hat{\Phi}(\vec{q})|^2 \right]. \quad (3.56)$$

To examine the effect of the density field onto the surface a simple approach is to integrate out the degrees of freedom related to the density field in the partition function

$$Z_G = \int D\hat{h} e^{-\mathcal{H}_{sur,\hat{h}}} \int D\hat{\Phi} e^{-\mathcal{H}_{sur,\hat{\Phi}}} \quad (3.57)$$

with

$$\mathcal{H}_{sur,\hat{h}}[\hat{h}] = \frac{1}{2} \int \frac{d\vec{q}}{(2\pi)^d} k q^4 |\hat{h}(\vec{q})|^2, \quad (3.58)$$

and

$$\mathcal{H}_{sur,\hat{\Phi}}[\hat{h}, \hat{\Phi}] = \frac{1}{2} \int \frac{d\vec{q} d\vec{q}'}{(2\pi)^d} (a + b q^2) \hat{\Phi}(\vec{q}) \hat{\Phi}(\vec{q}') \delta(\vec{q} + \vec{q}') + \int \frac{d\vec{q}}{(2\pi)^d} (-\mu q^2) \hat{\Phi}(\vec{q}) \hat{h}(-\vec{q}). \quad (3.59)$$

The functional integration in the density field in Eq.(3.57) amounts to a Gaussian functional integration and thus it can be carried out exactly. We identify the linear operator in the quadratic term and its inverse as

$$K(\vec{q}, \vec{q}') = \frac{a + b q^2}{(2\pi)^d} \delta(\vec{q} + \vec{q}') \quad K'(\vec{q}, \vec{q}') = \frac{(2\pi)^d}{a + b q^2} \delta(\vec{q} + \vec{q}'). \quad (3.60)$$

We obtain

$$\int D\hat{\Phi} e^{-\mathcal{H}_{sur,\hat{\Phi}}} = N \exp \left[-\frac{1}{2} \int \frac{d\vec{q}}{(2\pi)^d} \frac{\mu^2 q^4}{a + b q^2} |\hat{h}(\vec{q})|^2 \right], \quad (3.61)$$

which, inserting back in Eq.(3.57), leads to a partition function depending only on the height field, and an effective Hamiltonian

$$\mathcal{H}_{eff}[\hat{h}] = \frac{1}{2} \int \frac{d\vec{q}}{(2\pi)^d} q^4 \left[k - \frac{\mu^2}{a + b q^2} \right] |\hat{h}(\vec{q})|^2. \quad (3.62)$$

This introduces an effective bending rigidity

$$k_{eff} = k - \frac{\mu^2}{a + b q^2}, \quad (3.63)$$

which, if we restrict to large scale configurations reduces to

$$k_{eff} = k - \frac{\mu^2}{a}. \quad (3.64)$$

So, in the presence of diffusing particles, coupled to the surface spontaneous curvature, the bending rigidity decreases. Furthermore it can already be observed from this simple treatment that if $\mu^2 \rightarrow ak$ a **curvature instability** is present, in which the bending energy is renormalized to negative values. A more complete

treatment of this phenomenon can be found in [23].

We stress that the energy describing the diffusing particles onto the surface introduced in this section is **not** related to the self-aggregation phenomenon described in Chapter 2, which is a nonequilibrium phenomenon for which a functional cannot be introduced so easily. Nevertheless we will see in Chapter 5 that the numerical analysis of the model of self-aggregating particles coupled to the surface spontaneous curvature leads to some results that are in qualitative agreement with the ones explained in this section.

Chapter 4

Dynamically Triangulated Monte Carlo

Triangulated Monte Carlo methods have been first used in a membrane context to describe the crumpling transition of self avoiding tethered surfaces [25], with a static triangulation. Fluid membranes were first studied by Ho and Baumgartner [9, 26], using dynamically triangulated Monte Carlo (DTMC), in which the triangulation map of the surface is dynamic. The surface is discretized into a set of N vertices, T triangles and L links, with a surface topology defined by the Euler number $\chi = N + T - L$. Below a technique first proposed by Ramakrishnan et al.[11] to calculate the principal curvatures on triangulated surfaces is explained.

4.1 Triangulated Surface Model

To obtain the principal curvatures at vertices the procedure proposed in [10] and in [11] was followed. The curvature at vertex is calculated using its one-ring neighborhood, showed in Fig.4.2, and calculating the discretized shape operator, which contains all information about the local topography. The set of edges neighboring the considered vertex v are denoted as $\{e\}_v$, the set of oriented faces as $\{f\}_v$, and together they define the one-ring neighborhood. Similarly the set of faces neighboring an edge is described by $\{f\}_e = [f_1(e), f_2(e)]$.

Edge and Vertex normals:

Edge normals are completely determined by the set of their neighboring faces $\{f\}_e$ as

$$\hat{N}_e = \frac{\hat{N}_f(1, e) + \hat{N}_f(2, e)}{|\hat{N}_f(1, e) + \hat{N}_f(2, e)|}. \quad (4.1)$$

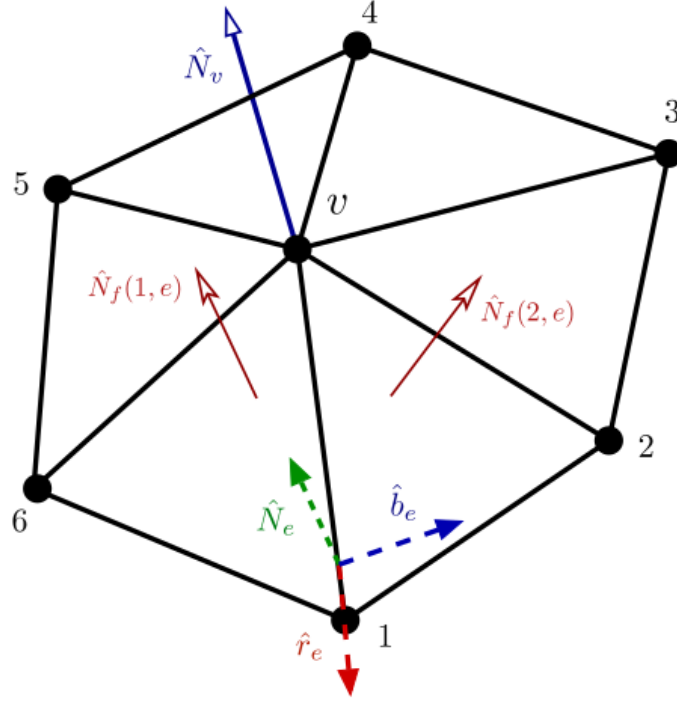


Figure 4.1: $\vec{r}_e = \vec{x}_v - \vec{x}_1$ is the vector along the edge connecting v to its neighbour, $\hat{N}_f(i, e)$ with $i = 1, 2$ are the face normals adjacent to the edge considered, \hat{N}_v is the normal at the vertex. \hat{N}_e and $\hat{b}_e = \hat{r}_e \times \hat{N}_e$ are respectively the edge normal and the binormal, with $\hat{r}_e = \frac{\vec{r}_e}{|\vec{r}_e|}$. Image taken from [10]

In the vertex normal definition instead there is an ambiguity. Denoting as \mathcal{S} a continuous surface around the vertex v and \mathcal{C} a closed contour on \mathcal{S} containing v , the vertex normal can be defined as:

$$N_v = \int_{\mathcal{C}} \hat{N}_{\mathcal{S}}(\mathcal{C}) d\mathcal{C} \quad (4.2)$$

with $\hat{N}_{\mathcal{S}}(\mathcal{C})$ the surface normal on the contour. When replacing the continuous surface \mathcal{S} with a discrete triangulated surface the surface normal only changes at the interface between faces, when the contour crosses an edge. This has to be accounted in the discrete version of Eq.(4.2) assigning an appropriate weight to each face contained in $\{f\}_v$. The mentioned ambiguity is in the choice of the weight. In this work the approach from [10] was followed, choosing a weight $\Omega[A]$ for the face normal proportional to the corresponding face area, obtaining the following

approximation:

$$\hat{N}_v = \frac{\sum_{\{f\}_v} \hat{N}_f \Omega[A_f]}{|\sum_{\{f\}_v} \hat{N}_f \Omega[A_f]|}, \quad (4.3)$$

with A_f the area of the face f .

Edge Shape operator:

The surface topographic details are contained in the faces and edges. The shape operator, the discrete counterpart of the curvature tensor, is constructed at each edge, and then projected to obtain the shape operator at the vertex. As mentioned, an object crossing a discrete surface feels its curvature only when crossing an edge. At any point p on such edge an edge curvature can be defined, which is the gradient of the area vector of the triangles sharing e [27],[28],

$$h(e) = \nabla_p(\text{area}) \approx 2|\vec{r}_e| \cos\left(\frac{\phi(e)}{2}\right) \quad (4.4)$$

where $\phi(e)$ is the signed dihedral angle between the faces sharing e , given by:

$$\phi(e) = [(\hat{N}_f(1, e) \times \hat{N}_f(2, e)) \cdot \vec{r}_e] \arccos(\hat{N}_f(1, e) \cdot \hat{N}_f(2, e)) + \pi. \quad (4.5)$$

The edge curvature can be used to define the shape operator, which contains information both about the curvature and the orientation of the edge:

$$S_E(e) = h(e)[\hat{b}(e) \otimes \hat{b}(e)]. \quad (4.6)$$

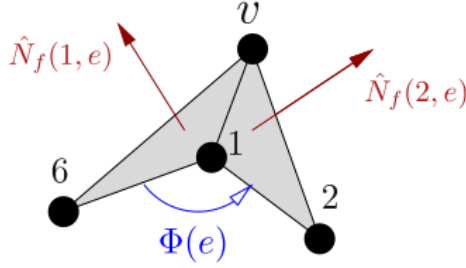


Figure 4.2: Illustration of dihedral angle, taken from [10]

Vertex Shape operator:

As was done on edges, the shape operator is constructed in the tangent plane at the vertex. The shape operator of every edge connected to a vertex contributes to the shape operator at the edge, so the shape operator at vertex $S_V(v)$ is a superposition of all the edge shape operators around it, $\{S_E(e)\}_v$. The relevant component of all

$S_E(e)$ is the one along the tangent plane at v , this can be obtained by defining the projection operator:

$$P_v = [\mathbb{I} - \hat{N}_V \otimes \hat{N}_V] \quad (4.7)$$

where \mathbb{I} is the identity matrix. The vertex shape operator can be expressed as a weighted sum of the projected shape operators:

$$S_V(v) = \frac{1}{A_V} \sum_{\{e\}_v} W(e) P_v^\dagger S_E(e) P_v, \quad (4.8)$$

where the weight factor is $W(e) = \hat{N}_v \cdot \hat{N}_e$, and $A_v = \sum_{\{f\}_v} A_f/3$ is the area assigned to each vertex. By definition the first two eigenvalues of the shape operator are the principal curvatures $c_1(v), c_2(v)$, with eigenvectors the principal curvature directions, and the third is zero with eigenvector along the vertex normal \hat{N}_v . The shape operator is defined in the global reference frame $[\hat{x}, \hat{y}, \hat{z}]$. To calculate the eigenvalues in a computationally convenient way a Householder transformation T_H can be used to rotate the \hat{z} axis to the normal vector \hat{N}_v , and obtain a 2×2 minor with as eigenvalues the principal curvatures. Calculating then the eigenvalues of the matrix in the rotated reference frame $C(v) = T_H(v)^\dagger S_V(v) T_H(v)$ is easier. Knowing the principal curvatures per vertex now the discretized version of the Helfrich hamiltonian can be written using the mean curvature per vertex $H_c(v) = \frac{1}{2}(c_1(v) + c_2(v))$, obtaining:

$$H_{el} = \frac{k}{2} \sum_{v=1}^N (c_1(v) + c_2(v))^2 A_v. \quad (4.9)$$

4.2 Monte Carlo Procedure

The equilibrium properties of the surface are described by its partition function:

$$Z(N, k) = \frac{1}{N!} \sum_{\{T\}} \prod_{v=1}^N \int d\vec{x}(v) \exp\{-\beta[H_{el}(\{\vec{X}\}, \{T\}) + V_{SA}]\}, \quad (4.10)$$

where V_{SA} is the self avoiding potential, here chosen as the hard sphere potential, \vec{X} is the position vector of all vertices of the surface, T the corresponding triangulation map. The integral is carried out over all possible vertices positions and summed over all possible triangulations. Imposing the hard sphere potential (i.e. prohibiting any configuration in which two vertices come closer than their diameter) and a maximum tether length $l = \sqrt{2}$ make the surface completely impenetrable, ensuring self avoidance [29]. See Fig.4.4 for clarity.

The state of the membrane in its phase space is described by the tuple $\eta =$

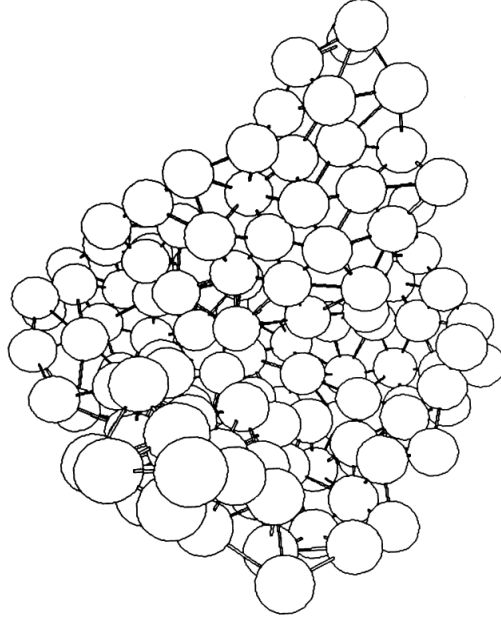


Figure 4.3: Representation of hard sphere potential with actual volumes of impenetrable beads [29].

$[\{\vec{X}\}, \{T\}]$. A Monte Carlo move corresponds to a change in the state of the system $\eta \rightarrow \eta'$, and it can be decomposed into two set of moves which both satisfy detailed balance.

(a) Vertex move:

The vertex positions are updated, $\{\vec{X}\} \rightarrow \{\vec{X}'\}$, moving a randomly chosen vertex in a cube of size 2σ around it. The triangulation map $\{T\}$ is left unchanged, so the system configuration changes as $\eta = [\{\vec{X}\}, \{T\}] \rightarrow \eta' = [\{\vec{X}'\}, \{T\}]$. The move must obey the detailed balance condition:

$$\omega(\eta \rightarrow \eta')P_{acc}(\eta \rightarrow \eta') = \omega(\eta' \rightarrow \eta)P_{acc}(\eta' \rightarrow \eta) \quad (4.11)$$

which, choosing for the forward and backward trial probabilities to be equal, and uniform in the choice of the vertex and the displacement

$$\omega(\eta \rightarrow \eta') = \omega(\eta' \rightarrow \eta) = \frac{1}{8N\sigma^3}, \quad (4.12)$$

gives for the acceptance probability the condition

$$P_{acc}(\eta \rightarrow \eta') = \min\{1, \exp[-\beta\Delta H_{el}(\eta \rightarrow \eta')]\}, \quad (4.13)$$

which is the usual Metropolis probability. The parameter σ determines the maximum displacement of vertices and thus the acceptance probability.

(a) Link flip:

An edge shared by two triangles is deleted, and another one connecting the two previously unconnected vertices is created. The triangulation map is updated $\{T\} \rightarrow \{T'\}$, and some vertices neighborhoods change, effectively creating a diffusion. The particle positions are left unchanged so the configuration changes as $\eta = [\{\vec{X}\}, \{T\}] \rightarrow \eta' = [\{\vec{X}\}, \{T'\}]$. The trial probability is given by $\omega(\eta \rightarrow \eta') = \omega(\eta' \rightarrow \eta) = \frac{1}{L}$, and applying the same reasoning with detailed balance the acceptance probability is the same as the vertex case.

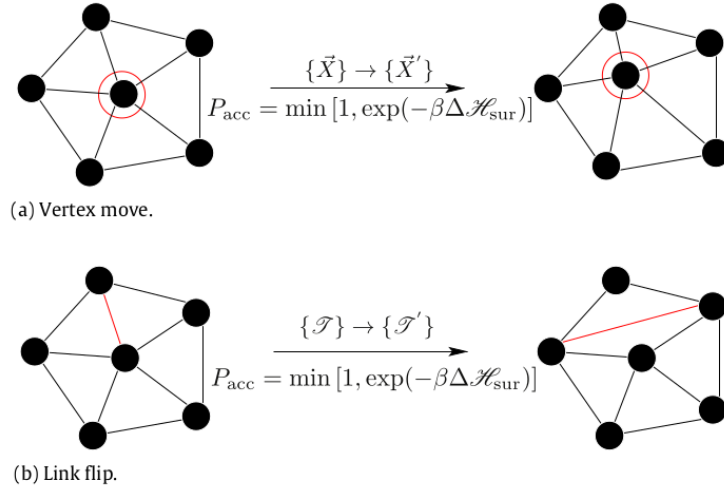


Figure 4.4: Monte Carlo moves for equilibrium simulation of a fluid random surface. (a) The vertex move simulates thermal fluctuations and (b) link flip simulates diffusion. [10]

Clearly the Monte Carlo moves must obey the conditions that ensure self avoiding, so all the moves that result in a tether length $l > \sqrt{2}$, or in a distance between vertices $d < 2r$ (where r is the radius of the hard spheres) are rejected. Finally, during the link flip dynamics the further condition that vertices cannot have less than 3 edges must be imposed, s.t. the total number of edges is conserved¹.

¹Without this condition edges can be deleted, due to the formation of pyramidal structures.

4.3 Technical Remarks

The naive way to implement this kind of procedure results in a computationally expensive algorithm, for two main reasons. The hard sphere potential requires that when any vertex is displaced it has to be checked that there is no overlapping with **all** other vertices, making the move $O(N^2)$. Furthermore, if the elastic energy is recalculated on the whole surface at each step, this results also in a $O(N^2)$ cost. This can be solved by making both calculations local:

- The overlapping check was solved using a Linked-List Cell structure, essentially dividing the space in cells, assigning each vertex to a cell, storing and then updating the positions during the dynamics. This allows to check only the vertices that are stored in neighboring cells for overlapping, making the procedure $O(1)$.
- The elastic energy calculation was done locally, updating after each vertex or link move only the curvatures associated to the interested vertices, and re-calculating it locally using the procedure explained in (4.1).

The algorithm implemented in this way is $O(N)$.

4.4 Coupling with particles

The idea is then to place particles evolving according to the Markov process explained in Sec.(2.4) onto the surface, considering an interaction between particles and surface, in which each particle creates a spontaneous curvature of the surface. The particles were inserted onto the triangular faces of the surface, such that the subsequent spontaneous curvature is localized first in the edges neighboring the occupied face. Then the contribution is projected onto the vertices curvatures.

Considering the discrete Hamiltonian describing the membrane in Eq.(4.9) and confronting it with the continuous version in (3.24) it's clear that until now we are describing a membrane with zero spontaneous curvature (which tends to be flat).

The shape operator at edges is defined by $S_e = h(e)\hat{b}(e) \otimes \hat{b}(e)$, with $h(e)$ a scalar measure of curvature at edge. We insert a coupling between particle presence and curvature in the following way: add a constant $-\mu$ to $h(e)$ if one adjacent face is occupied by a particle, -2μ if both. This way when particles are present the Shape operator is modified as: $S'_e = (h(e) - \alpha_e\mu)\hat{b}(e) \otimes \hat{b}(e)$, with $\alpha_e = 0,1,2$ an index associated to each edge, counting the number of neighboring faces occupied by particles. The trace of the new shape operator is $Tr(S'_e) = Tr(S_e)(1 - \alpha_e\mu)$.

Since the Shape operator at vertex is defined as the averaged sum of the projection

of the adjacent edge shape operators:

$$S_v = \frac{1}{A_v} \sum_{\{e\}} W(e) P^+(v) S_e P(v), \quad (4.14)$$

the eigenvalues are invariant under a change of basis, and the trace is linear, the trace of S_v is given by the weighted sum:

$$\text{Tr}(S_v) = \frac{1}{A_v} \sum_{\{e\}} W(e) \text{Tr}(S_e). \quad (4.15)$$

So, when particles are added edge shape operators are modified accordingly and shape operators at vertices change as:

$$\text{Tr}(S'_v) = \text{Tr}(S_v) - \sum_{\{e\}} \frac{\alpha_e \mu W(e) \text{Tr}(S_e)}{A_v}. \quad (4.16)$$

The trace of the shape operator at vertex is the mean curvature, so when particles are added, the mean curvature at the vertex changes as:

$$H'_c = H_c - \sum_{\{e\}} \frac{\alpha_e \mu W(e) \text{Tr}(S_e)}{A_v}. \quad (4.17)$$

Inserting this in the discrete form of the Helfrich Hamiltonian it becomes clear that this introduces a spontaneous curvature at each vertex proportional to the number of occupied neighbors, creating a coupling between the density of particles and the spontaneous curvature of the membrane.

4.5 Model Implementation

For the implementation, a geometry processing library, called **libigl** [30], was largely used. Following the structure introduced in such library, a triangulated surface with N vertices and T triangles is described simply as a pair of matrices

- *vertex list*, matrix of dimension $N \times 3$, i -th row contains the cartesian coordinates of the i -th vertex.
- *triangle list*, matrix of dimension $T \times 3$, i -th row contains the indices of the vertices forming the i -th triangle. The order of the vertex indices determines the face orientation, so it has to be consistent for the entire surface.

Various quantities describing the topography of the surface are initially calculated, and updated locally during the dynamics. The various functions are structured as

follows:

MC step vertex:

A random vertex is selected and displaced randomly inside a cube. It is checked that the self-avoiding conditions are satisfied by the new configurations, so that (1) the tethers connecting the displaced vertex with its neighbours onto the mesh don't exceed the maximum and (2) there is no overlapping of the hard spheres potential between that of the displaced vertex and of all the vertices assigned to one of the neighboring 26 cells of the Linked-List-Cell structure. If this is verified, the elastic energy of the new surface is calculated. This is done locally (to avoid an $O(N^2)$ cost), subtracting the curvature contribution associated to the old position of the vertex and the one associated to its neighbors, and recalculating them from their one-ring neighborhood according to the procedure explained in Sec.(4.1).

This allows to calculate the acceptance probability, if the move is accepted the quantities describing the surface (such as the Linked-List-Cell) are locally updated accordingly. Once this has been completed for all vertices (in random order) a sweep is complete.

MC step link:

A random edge is selected, and the vertices and edges related to the two triangles that share it are identified. Then the edge present in both triangles is removed, and an edge connecting the two remaining vertices is added. It is checked that the new edge length doesn't exceed the maximum, and that this operation does not lead to a vertex having less than three neighbors (that can happen due to the formation of pyramidal configurations that lead to the elimination of an edge, and superposed edges appearing multiple times). Furthermore the dynamics has to preserve the orientation of the faces, i.e. the order of the vertices.

If the conditions are satisfied, the elastic energy of the new configuration is calculated. This is again done locally, updating only the curvature contribution of the four vertices involved. If the move is then accepted the surface is updated accordingly. Once N tethers have undergone this procedure a sweep is complete.

Elastic Energy:

Both the initial energy calculation and the various local updates are performed according to the procedure explained in Sec.(4.1). When the energy is calculated onto the whole surface the shape operators at edges are stored in a list of matrices. This allows to avoid to recalculate these quantities when unnecessary, and speeds up the procedure. The different updates that have to be distinguished are the following

- *vertex update*: after a vertex is displaced, the orientation of all the neighboring faces changed. All the edge shape operators have to be recalculated.

- *neighborhood update*: update of curvature of the neighboring vertices of a displaced vertex. In their one-ring neighborhood only the edge shape operator associated to the edge connected to the displaced vertex has to be recalculated.
- *link update*: the shape operators of all the 5 edges involved and the related vertices have to be updated.

For all this different operations a specialized function was defined.

Particles:

Finally particles are inserted onto the surface, according to the Markov process presented in Sec.(2.4), and a coupling with surface spontaneous curvature is considered, as explained in Sec.(4.4).

Both for the insertion and diffusion process the surface curvature is updated locally after each move. For the extraction at each timestep all the clusters are individuated with a Depth First Search algorithm that finds the connected components. The energy is not updated immediately after the particle extraction, but is updated gradually during the subsequent vertex and link dynamics, in which the local curvature updates take into account the presence of the particles.

This choice was made both for simplicity and with the idea that an actual membrane would need a certain amount of time in which, after a vesicle extraction, it relaxes back to the original configuration.

The simulations performed in this work concern a surface with spherical topology. A typical configuration is shown in Fig.(4.5).

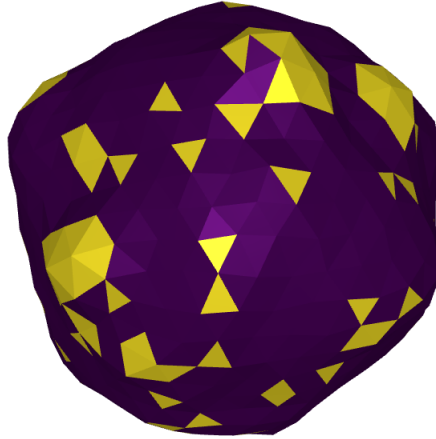


Figure 4.5: Example of a typical configuration, with $N = 642$, $k = 500$, $\mu = 0.5$, $k_I = 10^{-5}$, $k_D = 100$, $g = 250$, $N_E = 20$.

For the complete code see <https://github.com/giangomango/DTMC>.

Chapter 5

Results and Discussion

In the simulations time was measured in MCS (Monte Carlo Sweeps), and measures were taken in the stationary state, considering one configuration every 10 MCS. The ensemble average of the particle density in the stationary state was measured at different values of μ and k , to examine how the aggregation process is modified by the surface fluctuations. As can be seen in Fig.(5.1), it seems that the particle density is independent both from μ and k . The ensemble average of the elastic

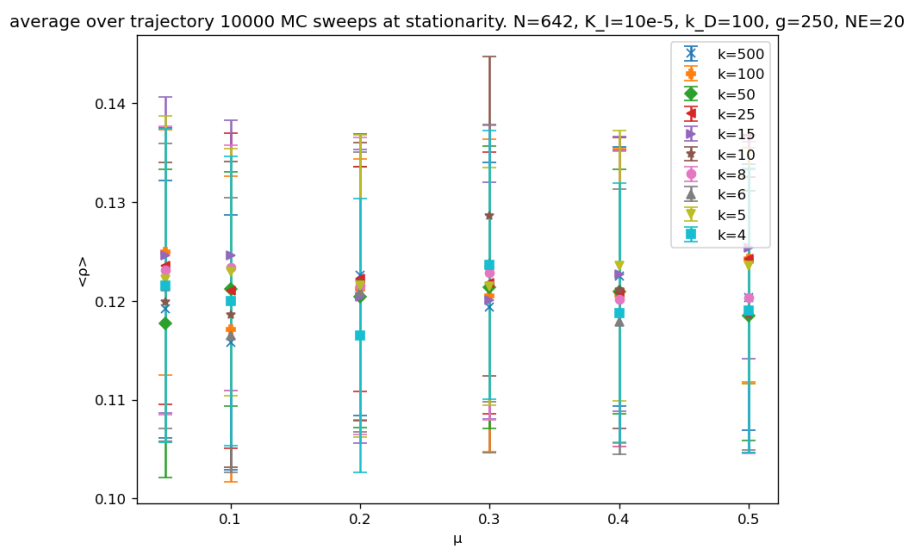


Figure 5.1: Stationary state ensemble average of the particle density.

energy in the stationary state was measured at different values of the particle-membrane coupling μ and the membrane bending energy k , as can be seen in Fig.(5.2).

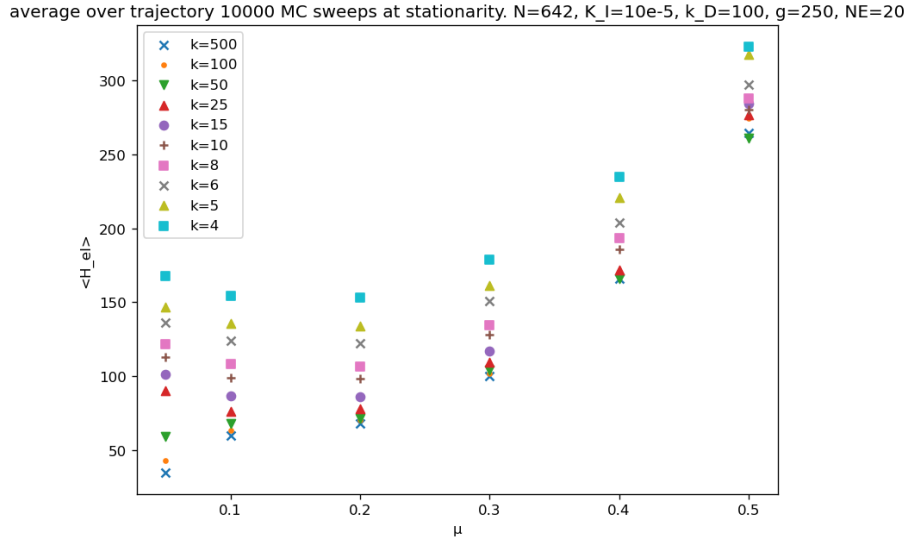


Figure 5.2: Stationary state ensemble average of the elastic energy.

It can be observed that beyond a certain value of the coupling μ the energy increases monotonically with it. This observation can be qualitatively linked with the renormalization of the bending energy to lower values by a factor proportional to the coupling μ presented in Sec.(3.5). The related model was introduced in an equilibrium context, of freely diffusing interacting particles, with a coupling with the surface spontaneous curvature, onto a fluid membrane. Despite the differences between this model and the one that is considered in this work (in which particles are inserted, undergo aggregation, and are extracted, keeping the system in a driven nonequilibrium state), the qualitative conclusion that the spontaneous curvature induced by the particles renormalizes the bending energy to smaller values is in agreement. Actually one relevant common element between the two models is the form of the interaction between the particles density and the spontaneous curvature.

The interaction introduced by Leibler [23] has the form

$$\mathcal{H}_{int} = - \int dS \mu \Phi H_c, \quad (5.1)$$

and, upon defining a local function calculating the local correction due to presence of particles

$$\Psi(v) = \sum_{\{e\}_v} \frac{\alpha_e W(e) Tr(S_e)}{A_v} \quad (5.2)$$

inserting the local correction introduced in our numerical model, Eq.(4.17), into the discrete form of the Helfich Hamiltonian we obtain

$$\begin{aligned} H_{el} &= \frac{k}{2} \sum_{v=1}^N (H_c - \mu \Psi(v))^2 A_v \\ &= \frac{k}{2} \sum_{v=1}^N (H_c^2 - 2\mu \Psi(v) H_c + \mu^2 \Psi(v)^2) A_v. \end{aligned} \quad (5.3)$$

A further comment can be made about the fact that for values of $k \geq 50$ the energy always increases w.r.t μ , even if with a small plateau. Instead, for values smaller there is an initial decrease. This means that there is a change in dependence of the energy from μ changing the bending modulus, signaling some change of regime. This could be related to the curvature instability introduced in [23, 24], with the difference that in this context the instability triggered by the particles is localized in specific regions. However, at this level this conclusion cannot be drawn, and this effect needs further investigation.

Finally, observing Figs.(5.2) and (5.3), we can see that as the coupling μ increases the bending modulus becomes less relevant in determining the elastic energy of the stationary configuration. In fact the energies for different k become closer and closer and the configurations become more similar. This suggest that a larger coupling value μ at which the bending modulus k becomes irrelevant could exist.

5.1 Domain Distance frequency density

In order to evaluate the distance frequency density for domains the following procedure was employed:

- The centroids of clusters were found taking the area weighted average of geometrical centers of single triangles belonging to the domain. Then the vertex belonging to the domain which is closest to the point found is selected as centroid.

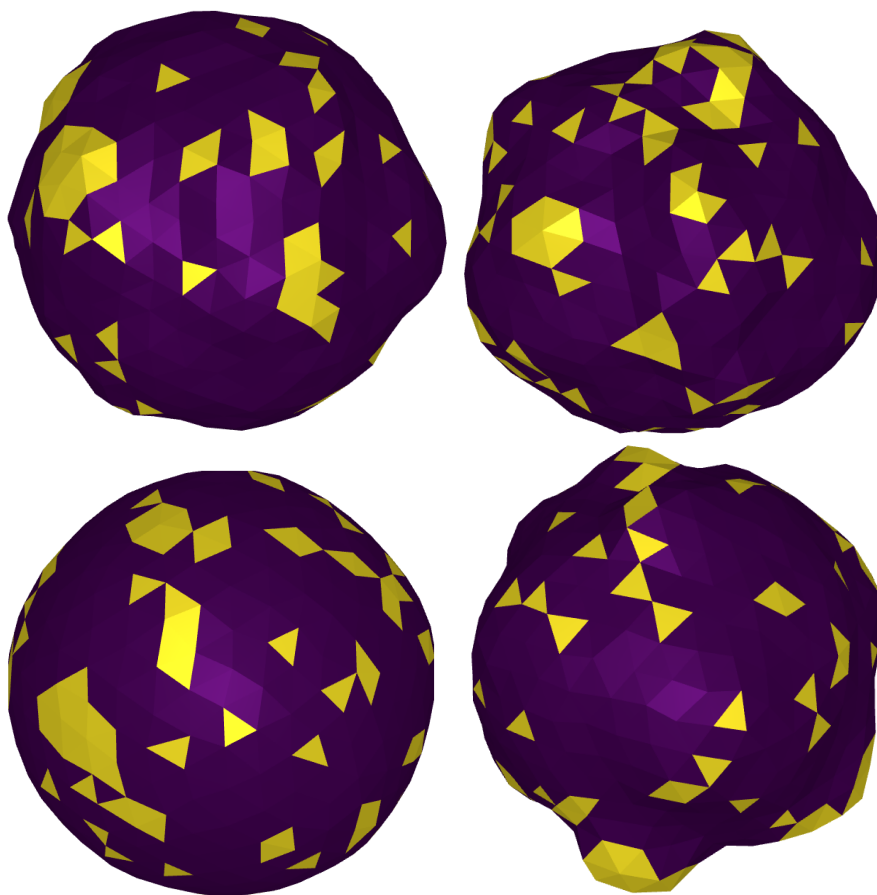


Figure 5.3: On the upper left configuration with $k = 4$, $\mu = 0.05$, upper right configuration with $k = 4$ and $\mu = 0.5$. Downward left $k = 500$, $\mu = 0.05$, downward right $k = 500$, $\mu = 0.5$. Clearly, at lower values of the coupling μ the elastic energy is more relevant in determining the behaviour of the system, as it can be seen confronting the figures on the left. Instead, when the coupling is big the bending modulus is less relevant, as it can be seen from the similarity of the figures on the right.

- Selecting as centroid a vertex allows to determine the distance between domains as a shortest path distance on a weighted graph. The graph has as nodes the vertices of the triangulated surface and as edges the tethers connecting the vertices. Then the distance is found employing Dijkstra's algorithm.

The result is shown in Fig.(5.4), where no particular dependence from μ or k is observed.

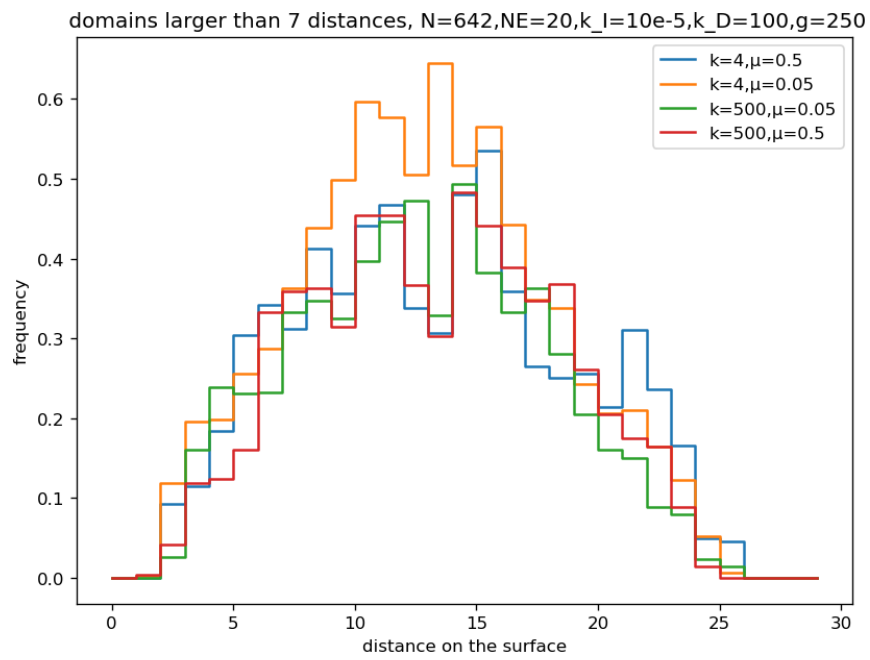


Figure 5.4: Frequency of domains distance distribution, varying k and μ .

Bibliography

- [1] Sara Sigismund, Stefano Confalonieri, Andrea Ciliberto, Simona Polo, Giorgio Scita, and Pier Paolo Di Fiore. «Endocytosis and Signaling: Cell Logistics Shape the Eukaryotic Cell Plan». In: *Physiological Reviews* 92.1 (2012). PMID: 22298658, pp. 273–366. DOI: 10.1152/physrev.00005.2011. eprint: <https://doi.org/10.1152/physrev.00005.2011>. URL: <https://doi.org/10.1152/physrev.00005.2011> (cit. on p. 1).
- [2] Ira Mellman and W Nelson. «Mellman I, Nelson WJ Coordinated protein sorting, targeting and distribution in polarized cells. Nat Rev Mol Cell Biol 9(11): 833-845». In: *Nature reviews. Molecular cell biology* 9 (Dec. 2008), pp. 833–45. DOI: 10.1038/nrm2525 (cit. on p. 1).
- [3] Marco Zamparo, Donatella Valdembri, Guido Serini, Igor V. Kolokolov, Vladimir V. Lebedev, Luca Dall’Asta, and Andrea Gamba. «Optimality in Self-Organized Molecular Sorting». In: *Phys. Rev. Lett.* 126 (8 Feb. 2021), p. 088101. DOI: 10.1103/PhysRevLett.126.088101. URL: <https://link.aps.org/doi/10.1103/PhysRevLett.126.088101> (cit. on pp. 1–3, 8).
- [4] Elisa Floris et al. *Phase separation and critical size in molecular sorting*. 2022. DOI: 10.48550/ARXIV.2205.03337. URL: <https://arxiv.org/abs/2205.03337> (cit. on pp. 1–3, 8, 9, 11).
- [5] Daniel Nunez, Costin Antonescu, Marcel Mettlen, Allen Liu, Sandra Schmid, Dinah Loerke, and Gaudenz Danuser. «Hotspots Organize Clathrin-Mediated Endocytosis by Efficient Recruitment and Retention of Nucleating Resources». In: *Traffic (Copenhagen, Denmark)* 12 (Aug. 2011), pp. 1868–78. DOI: 10.1111/j.1600-0854.2011.01273.x (cit. on p. 1).
- [6] W. Helfrich. «Elastic Properties of Lipid Bilayers: Theory and Possible Experiments». In: *Z. Naturforsch. C* 28 (Dec. 1973). DOI: 10.1515/znc-1973-11-1209 (cit. on pp. 1, 19).
- [7] David R. Nelson, Tsvi Piran, and Steven Weinberg. «Statistical mechanics of membranes and surfaces». In: 2004 (cit. on pp. 1, 19, 21).

-
- [8] Markus Deserno. «Fluid lipid membranes – a primer». In: 2006 (cit. on pp. 1, 19).
- [9] J.-S Ho and A Baumgärtner. «Simulations of Fluid Self-Avoiding Membranes». In: *Europhysics Letters (EPL)* 12.4 (June 1990), pp. 295–300. DOI: 10.1209/0295-5075/12/4/002. URL: <https://doi.org/10.1209/0295-5075/12/4/002> (cit. on pp. 1, 28).
- [10] N. Ramakrishnan, P.B. Sunil Kumar, and Ravi Radhakrishnan. «Mesoscale computational studies of membrane bilayer remodeling by curvature-inducing proteins». In: *Physics Reports* 543.1 (2014). Mesoscale computational studies of membrane bilayer remodeling by curvature-inducing proteins, pp. 1–60. ISSN: 0370-1573. DOI: <https://doi.org/10.1016/j.physrep.2014.05.001>. URL: <https://www.sciencedirect.com/science/article/pii/S0370157314002038> (cit. on pp. 1, 14, 28–30, 33).
- [11] N. Ramakrishnan, P. B. Sunil Kumar, and John H. Ipsen. «Monte Carlo simulations of fluid vesicles with in-plane orientational ordering». In: *Phys. Rev. E* 81 (4 Apr. 2010), p. 041922. DOI: 10.1103/PhysRevE.81.041922. URL: <https://link.aps.org/doi/10.1103/PhysRevE.81.041922> (cit. on pp. 1, 28).
- [12] N. Ramakrishnan, P. B. Sunil Kumar, and John H. Ipsen. «Modeling Anisotropic Elasticity of Fluid Membranes». In: *Macromolecular Theory and Simulations* 20.7 (June 2011), pp. 446–450. DOI: 10.1002/mats.201100002. URL: <https://doi.org/10.1002/mats.201100002> (cit. on p. 1).
- [13] D. M. Kroll and G. Gompper. «Scaling behavior of randomly triangulated self-avoiding surfaces». In: *Phys. Rev. A* 46 (6 Sept. 1992), pp. 3119–3122. DOI: 10.1103/PhysRevA.46.3119. URL: <https://link.aps.org/doi/10.1103/PhysRevA.46.3119> (cit. on p. 1).
- [14] G. Gompper and D. M. Kroll. «Phase diagram and scaling behavior of fluid vesicles». In: *Phys. Rev. E* 51 (1 Jan. 1995), pp. 514–525. DOI: 10.1103/PhysRevE.51.514. URL: <https://link.aps.org/doi/10.1103/PhysRevE.51.514> (cit. on p. 1).
- [15] Pavel L. Krapivsky, Sidney Redner, and Eli Ben-Naim. *A Kinetic View of Statistical Physics*. Cambridge University Press, 2010. DOI: 10.1017/CB09780511780516 (cit. on pp. 3, 4, 6, 7).
- [16] «Kinetics of Nucleation–Growth Processes: The First Stages». In: *Kinetics of First-Order Ph*. John Wiley and Sons, Ltd, 2009. Chap. 3, pp. 39–91. ISBN: 9783527627769. DOI: <https://doi.org/10.1002/9783527627769.ch3>. eprint: <https://onlinelibrary.wiley.com/doi/pdf/10.1002/9783527627769.ch3>. URL: <https://onlinelibrary.wiley.com/doi/abs/10.1002/9783527627769.ch3> (cit. on p. 9).

- [17] P. M. Chaikin and T. C. Lubensky. *Principles of Condensed Matter Physics*. Cambridge University Press, 1995. DOI: 10.1017/CB09780511813467 (cit. on pp. 14, 15, 17, 18, 21).
- [18] L. Peliti. «Effective rigidity of membranes». In: *Physica A: Statistical Mechanics and its Applications* 140.1 (1986), pp. 269–277. ISSN: 0378-4371. DOI: [https://doi.org/10.1016/0378-4371\(86\)90231-1](https://doi.org/10.1016/0378-4371(86)90231-1). URL: <https://www.sciencedirect.com/science/article/pii/0378437186902311> (cit. on pp. 19, 25).
- [19] P. G. De Gennes and C. Taupin. «Microemulsions and the flexibility of oil/water interfaces». In: *The Journal of Physical Chemistry* 86.13 (1982), pp. 2294–2304. DOI: 10.1021/j100210a011. eprint: <https://doi.org/10.1021/j100210a011>. URL: <https://doi.org/10.1021/j100210a011> (cit. on p. 21).
- [20] L. Peliti and S. Leibler. «Effects of Thermal Fluctuations on Systems with Small Surface Tension». In: *Phys. Rev. Lett.* 54 (15 Apr. 1985), pp. 1690–1693. DOI: 10.1103/PhysRevLett.54.1690. URL: <https://link.aps.org/doi/10.1103/PhysRevLett.54.1690> (cit. on p. 21).
- [21] Mehran Kardar. *Statistical Physics of Fields*. Cambridge University Press, 2007. DOI: 10.1017/CB09780511815881 (cit. on p. 22).
- [22] Markus Deserno. «The influence of thermal fluctuations on the bending rigidity of fluid membranes». In: (cit. on p. 22).
- [23] S. Leibler. «Curvature instability in membranes». In: *Journal de Physique* 47.3 (1986), pp. 507–516. DOI: 10.1051/jphys:01986004703050700. URL: <https://hal.archives-ouvertes.fr/jpa-00210231> (cit. on pp. 25, 27, 40).
- [24] S. Leibler and David Andelman. «Ordered and curved meso-structures in membranes and amphiphilic films». In: <http://dx.doi.org/10.1051/jphys:0198700480110201300> 48 (Nov. 1987). DOI: 10.1051/jphys:0198700480110201300 (cit. on pp. 25, 40).
- [25] Yacov Kantor, Mehran Kardar, and David R. Nelson. «Statistical Mechanics of Tethered Surfaces». In: *Phys. Rev. Lett.* 57 (7 Aug. 1986), pp. 791–794. DOI: 10.1103/PhysRevLett.57.791. URL: <https://link.aps.org/doi/10.1103/PhysRevLett.57.791> (cit. on p. 28).
- [26] A. Baumgärtner and J.-S. Ho. «Crumpling of fluid vesicles». In: *Phys. Rev. A* 41 (10 May 1990), pp. 5747–5750. DOI: 10.1103/PhysRevA.41.5747. URL: <https://link.aps.org/doi/10.1103/PhysRevA.41.5747> (cit. on p. 28).
- [27] Konrad Polthier. «Polyhedral Surfaces of Constant Mean Curvature». In: 2002 (cit. on p. 30).

- [28] Keenan Crane, Fernando de Goes, Mathieu Desbrun, and Peter Schröder. «Discrete Differential Geometry: An Applied Introduction». In: 2013 (cit. on p. 30).
- [29] Yacov Kantor, Mehran Kardar, and David R. Nelson. «Tethered surfaces: Statics and dynamics». In: *Phys. Rev. A* 35 (7 Apr. 1987), pp. 3056–3071. DOI: 10.1103/PhysRevA.35.3056. URL: <https://link.aps.org/doi/10.1103/PhysRevA.35.3056> (cit. on pp. 31, 32).
- [30] Alec Jacobson, Daniele Panozzo, et al. libigl: A simple C++ geometry processing library. <https://libigl.github.io/>. 2018 (cit. on p. 35).